Title

# Antagonistic regulation of gibberellin response during growth of rice stem

Keisuke Nagai[1], Yoshinao Mori[2], Shin Ishikawa[2], Tomoyuki Furuta[1,3], Rico Gamuyao[1], Yoko Niimi[1], Tokunori Hobo[1], Moyuri Fukuda[2], Mikiko Kojima[4], Yumiko Takebayashi[4], Atsushi Fukushima[4], Yasuyo Himuro[5], Masatomo Kobayashi[5], Wataru Ackley[6], Hiroshi Hisano[3], Kazuhiro Sato[3], Aya Yoshida[7], Jianzhong Wu[8], Hitoshi Sakakibara[2], Yutaka Sato[9], Hiroyuki Tsuji[7], Takashi Akagi[10] and Motoyuki Ashikari[1]

**Affiliations**

[1] Bioscience and Biotechnology Center, Nagoya University, Aichi, Japan

[2] Graduate School of Bioagricultural Sciences, Nagoya University, Aichi, Japan

[3] Institute of Plant Science and Resources, Okayama University, Okayama, Japan

[4] RIKEN Center for Sustainable Resource Science, Kanagawa, Japan

[5] RIKEN BioResource Center, Ibaraki, Japan

[6] Institute of Livestock and Grassland Science, NARO, Tochigi, Japan

[7] Kihara Institute for Biological Research, Yokohama City University, Kanagawa, Japan

[8] Institute of Crop Science, NARO, Ibaraki, JAPAN

[9] National Institute of Genetics, Shizuoka, Japan

[10] Graduate School of Environmental and Life Science, Okayama University, Okayama, Japan

Corresponding author: Motoyuki Ashikari <ashi@agr.nagoya-u.ac.jp>

## Summary

**Plant stem growth largely determines plant size. Stem elongation is stimulated and promoted by gibberellic acid (GA)[1-3]. Here we demonstrate the antagonistic regulation of rice stem (internode) elongation by an "accelerator" and a "decelerator" in concert with GA. The gene *ACCELERATOR OF INTERNODE ELONGATION1* (*ACE1*), which encodes a protein of**

**unknown function, confers competence for cell division of intercalary meristematic region leading to internode elongation in the presence of GA. On the contrary, *DECELERATOR OF INTERNODE ELONGATION1* (*DEC1*), which encodes a zinc-finger transcription factor, suppresses internode elongation while downregulation of *DEC1* allows internode elongation. We also show that the mechanism of internode elongation mediated by *ACE1* and *DEC1* is conserved in Gramineae. Furthermore, genetic diversity analysis suggests that mutations in *ACE1* and *DEC1* had historically contributed to the selection of shorter plants for lodging resistance in domesticated populations and of taller plants for deepwater adaptation in wild species of rice. These antagonistic regulatory factors enhance our understanding of the GA response as an additional mechanism regulating internode elongation and environmental fitness beyond biosynthesis and GA signal transduction.**

## Main

The stem is a primary structural axis of plants that supports the aerial organs such as leaves and flowers. Stem elongation enables plants to adapt and survive in their environment. For example, elongated stems keep the leaves exposed to light, thereby maximizing photosynthetic efficiency[4]. In gramineous plants, the stem, which is composed of nodes and internodes, impacts plant height and productivity. Internode elongation is stimulated by the plant hormone gibberellic acid (GA) through the activation of cell division and cell elongation[1-3]. Regulation of internode length is an important target trait in crop breeding. In the two major crops, rice and wheat, semi-dwarf varieties with shorter internodes caused by reduced GA biosynthesis or signal transduction have been produced and are widely cultivated worldwide[5,6]. In contrast, the flood-resistant rice, known as deepwater (DW) rice which elongates internode according to water depth, survives periodic, deep and long-duration flooding in South Asia

and West Africa[7]. Previously, we demonstrated that the DW-induced expression and high enzymatic activity of GA20ox2, a protein involved in GA biosynthesis, promotes internode elongation in DW rice[8]. In a different aspect of internode elongation by GA, the internode requires activation of the intercalary meristem to initiate the elongation[9-11](Extended Data Fig. 1, SI.1). However, the regulatory factors and molecular mechanism of the GA response and intercalary meristem activity are unknown. To fill the gaps between the GA response and acquisition of the ability for internode elongation, we identified the factors controlling internode elongation in response to GA. Here we report the identities of two such factors, which operate by accelerating and decelerating the initiation of internode elongation alongside GA accumulation.

**Internode-specific gibberellic acid response**

DW rice (*O*ryza *sativa*, admixture, C9285[8]) grows taller than normal paddy rice (*O. sativa* subsp. *japonica* cv. Taichung 65: T65) under shallow water (SW) conditions (normal irrigation with ~5-cm-deep water) (Fig. 1a, b and Extended Data Fig. 2a). This vigorous growth depends on internode elongation (Fig. 1c). In T65, internode elongation was suppressed during the vegetative phase, and was observed only at around the 11-leaf stage during the transition from vegetative to reproductive phase (Fig. 1c and Extended Data Fig. 2b, 3a). In contrast, C9285 showed internode elongation even at the vegetative phase (6-leaf stage) without transition to the reproductive phase (Fig. 1c and Extended Data Fig. 2b, 3b). Under SW conditions, the final plant height, internode length, and number of elongated internodes of C9285 were greater than T65 (Extended Data Figs. 2c-e). Under DW conditions (120-cm-deep water), internode elongation was enhanced at the early vegetative phase (4-leaf stage) in C9285, but not in T65 (Fig. 1c and Extended Data Fig. 3a, b). As endogenous GAs regulate plant growth[12], we quantified endogenous GA in C9285 and T65 under SW and DW

conditions. Although GA accumulation in C9285 did not increase markedly under SW conditions, internode elongation was initiated at the vegetative stage (Fig. 1c and Extended Data Fig. 2f, SI.2). Next, we investigated the growth response of leaves and internodes to exogenous GA treatment. The length of the second leaf sheath of both varieties showed similar dose-dependent elongation in response to GA (Fig. 1d-f). Intriguingly, the internode elongation response differed significantly between the two varieties. The internodes of T65 did not elongate even at high GA concentrations, whereas C9285 internodes showed elongation in a GA concentration- and time-dependent manner (Fig. 1d-g, Extended Data Fig. 2g, Supplementary video). GA did not increase the total number of internodes in T65 and C9285 but did increase the number of elongated internodes in C9285 (Extended Data Fig. 2h). We tested whether exogenous GA promotes internode elongation of T65 and C9285 under DW conditions (Extended Data Fig. 3c, SI.3). Internode elongation of C9285 was observed with GA treatment or DW conditions alone and was further enhanced by their combination (Fig. 1h). However, the internodes of T65 did not respond to any conditions. Furthermore, we confirmed the degradation of SLR1, a key inhibitor of GA signaling degraded by the $SCF^{GID1}$ system in the presence of $GA^{12}$, in the internodes of T65 and C9285 under exogenous GA treatment. Although there were differential internode elongation responses to GA of T65 and C9285, the degradation of SLR1 in the internode of both genotypes was comparable (Extended Data Fig. 2i). Overall, these results suggest the presence of internode-specific factor(s) that promote or repress internode elongation in rice, in concert with GA accumulation, which may function downstream of GA signaling at the vegetative phase.

**Evaluation of QTLs related to GA response**

We previously performed a quantitative trait locus (QTL) analysis for the internode elongation in response to GA and detected 5 QTLs[13](Extended Data Fig. 3d). Two major QTLs on chromosomes 3 and 12 overlapped with QTLs regulating the initiation of internode elongation under DW conditions[14](Extended Data Fig. 3d). The factors controlling the initiation of internode elongation have not been identified[10,15]. To elucidate the effects of QTLs on chromosomes 3 and 12, we evaluated the internode elongation of near-isogenic lines (NILs) in response to exogenous GA treatment (Fig. 2a, Extended Data Fig. 3e). NIL3 and NIL12 showed internode elongation from 3 and 4 weeks after GA treatment of germinating seeds, respectively. In contrast, the normal paddy rice T65 did not show such a response. The QTL-pyramiding line NIL3+12 exhibited earlier and more enhanced internode elongation than NIL3 and NIL12, suggesting that the causal genes on chromosomes 3 and 12 regulate internode elongation independently. Moreover, we investigated the relationship of QTLs on chromosomes 3, 12 and *GA20ox2*, the causal gene of chromosome 1 QTL in DW rice (Extended Data Fig. 3f, g, SI.4). Overall, our results indicate that at least two factors accelerate internode elongation in response to GA, on chromosomes 3 and 12 of C9285, and that they function additively.

**ACE1 accelerates internode elongation**

We performed positional cloning to identify the responsible gene on chromosome 3 controlling internode elongation via GA. A high-resolution linkage analysis narrowed down the candidate region to < 1 kilobase pair containing only one putative gene, which we named *ACCELERATOR OF INTERNODE ELONGATION1* (*ACE1*) (Fig. 2b, Extended Data Fig. 3h). The allele from C9285 exerted the dominant effect on internode elongation in response to GA (Extended Data Fig. 3i, j). Furthermore, this allele also enhanced the DW response (Extended Data Fig. 3k, l), suggesting that the same genes mediate the GA and DW responses. Comparison of the *ACE1* sequences of T65 and C9285

revealed a 1 bp indel in the coding sequence (Fig. 2b and Extended Data Fig. 4a, b). Therefore, *ACE1*$^{T65}$ or *ACE1*$^{C9285}$ must be functional. To identify which allele is functional, we performed a gain-of-function analysis by introducing a genomic fragment of *ACE1* region of T65 or C9285 into the T65. Transgenic plants harboring the *ACE1* genomic fragment of C9285 (g*ACE1*$^{C9285}$) showed significant internode elongation in response to GA, but g*ACE1*$^{T65}$ did not (Fig. 2c, d). A 5′-RACE analysis detected two types of transcript isoforms (long and short) in C9285 and T65 (Extended Data Fig. 4c, d). Although the overexpressor of long *ACE1*$^{C9285}$ (*ACE1*$^{C9285}$ox) transcript did not show internode elongation in the absence of GA (Extended Data Fig. 4e, f), application of exogenous GA substantially induced internode elongation of *ACE1*$^{C9285}$ox, independent of the reproductive phase transition (Extended Data Fig. 4e-g). However, the overexpressor of long *ACE1*$^{T65}$ (*ACE1*$^{T65}$ox) transcript did not show internode elongation in the presence or absence of GA (Extended Data Fig. 4e, f). In addition, the overexpressor of short *ACE1* (*ACE1*$^{short}$ox) transcript of T65 and C9285, which has identical amino acid sequences from 33 to end of ACE1$^{C9285}$(Extended Data Fig. 4c, d), also did not elongate (Extended Data Fig. 4h, i). Introduction of *ACE1*$^{C9285}$ to NIL12, NIL1+3+12, and C9285 induced extensive internode elongation with lateral orientation of the base of internodes (Fig. 2e and Extended Data Fig. 4j-n). We conclude that long *ACE1*$^{T65}$ transcript and short transcripts do not have function while the long ACE1$^{C9285}$ protein (full-length amino acid sequence) is functional and essential for internode elongation, independently of the transition to the reproductive phase.

Under GA treatment or DW conditions, *ACE1*$^{C9285}$ expression was induced whereas *ACE1*$^{T65}$ expression was relatively low (Fig. 2f, g). *ACE1*$^{C9285}$ was mainly expressed in the elongating internodes, particularly in cell elongation zone rather than in cell division zone (Extended Data Fig. 5). While *ACE1*$^{T65}$ expression was low in T65 at all growth stages, *ACE1*$^{C9285}$ expression in C9285 increased at the 6-leaf stage under SW conditions, coinciding with the initiation of internode

elongation (Fig. 2h, i). Under DW conditions, *ACE1*$^{C9285}$ expression and internode elongation in C9285 were induced at the 4-leaf stage (Fig. 2h, i). *ACE1* expression correlated with the initiation of internode elongation in C9285 under SW and DW conditions. Trans-eQTL analysis and transgenic plant experiment revealed that SUB1C is one of the factors regulating *ACE1* expression (Extended Data Fig. 6a-g, SI.5, Supplementary Table 1). Taken together, these results conclude that *ACE1*$^{C9285}$ is a genetic determinant of the initiation of internode elongation in response to GA.

**ACE1 stimulates intercalary meristem with GA**

The ACE1$^{T65}$-GFP was detected preferentially in the nucleus, while the ACE1$^{C9285}$-GFP protein localized to the nucleus and cytosol (Extended Data Fig. 4b, 6h). To investigate the tissue localization of ACE1$^{C9285}$, we conducted immunostaining using an anti-ACE1$^{C9285}$ antibody (Extended Data Fig. 7a). ACE1$^{C9285}$ was localized in elongating internodes under GA treatment and DW conditions (Fig. 3a-d and Extended Data Fig. 7b-i). After 10 days, ACE1$^{C9285}$ was localized at the base of elongating internode under GA treatment and DW conditions (about 2 to 10 mm above the node) (Extended Data Fig. 7c-e, h, i). Next, we performed expression analyses to assess the role of *ACE1* in internode elongation. *ACE1*$^{C9285}$ overexpression or exogenous GA alone was not sufficient to activate the expression of genes associated with cell division (*Histone H4* and *CDKA1*) in internodes. However, *ACE1*$^{C9285}$ overexpression in concert with GA increased the expression of *Histone H4* and *CDKA1* (Fig. 3e). We next monitored the cell division status at the internodes using the S-phase-specific DNA synthesis marker, EdU to visualize the cell division region[16](Extended Data Fig. 8a-e). The application of exogenous GA to *ACE1*$^{C9285}$ox induced cell division and resulted in an enlarged cell division zone (Extended Data Fig. 8f). Furthermore, cell division of *ACE1*$^{C9285}$ox was maintained at the basal region of the internode, where the intercalary meristem has been reported to be located[3], resulting in

elongation of internodes (Extended Data Fig. 8f, g). In the control plants (VC), cells at the early stage of internode development also divided, although this division was not maintained and, as a result, the internodes did not elongate (Extended Data Fig. 8f, g). The results indicate that *ACE1*$^{C9285}$ may be related to activation and maintenance of the intercalary meristem in internodes, as *ACE1*$^{C9285}$ confers cell division competency by increasing GA responsiveness (Extended Data Fig. 8h, i).

**_ACE1-LIKE1_ facilitates internode elongation**

We retrieved the full-length amino acid sequences of *ACE1*$^{C9285}$ homologs and performed a phylogenetic analysis. *ACE1*$^{C9285}$ homologs are present in a wide range of species from moss to angiosperms and possess three conserved motifs of unknown function (Extended Data Figs. 9a-e, Supplementary Table 2). One of the *ACE1*$^{C9285}$ homologs in *Arabidopsis* has been reported as *FLOWERING PROMOTING FACTOR1* (*FPF1*)[17](Extended Data Fig. 9d, f). We found that T65 does not have a functional *ACE1* allele, but the T65 was capable of internode elongation at the reproductive phase (Fig. 1c), indicating that *ACE1* homolog(s) may be present in the genome of normal paddy rice, and promote internode elongation. Among the six rice homologs, *LOC_Os07g47450* (*ACE1-LIKE1* [*ACL1*]) showed the highest homology to *ACE1*$^{C9285}$ (Fig. 3f and Extended Data Fig. 9a, g). Under SW conditions, T65 showed lower *ACE1* expression whereas *ACL1* expression was upregulated at the 7-leaf stage (Fig. 3g). T65 at the 7-leaf stage did not show internode elongation, but exogenous GA treatment promoted internode elongation (Fig. 3h). Furthermore, T65 showed elevated *ACL1* expression at the 12-leaf stage and induced internode elongation without exogenous GA treatment (Fig. 3g, h). The expression pattern of *ACL1* is consistent with transition to reproductive phase in T65 (Fig. 3g and Extended Data Fig. 2b). In addition, the normal paddy rice Nipponbare showed similar expression pattern (Extended Data Fig. 9h), further suggesting that *ACL1* expression overlaps with the

vegetative to reproductive phase transition. Similar to *ACE1*$^{C9285}$ox plants, overexpression of *ACL1* in T65 genetic background resulted in internode elongation and an increase in the total internode length both in 3-week old seedlings and in mature plants (Fig. 3i-k). In contrast, *acl1* mutant plants generated using CRISPR/Cas9 did not show defective internode elongation but exhibited a decreased final internode length in T65 (Extended Data Fig. 9i-k). As *acl1* mutant plants showed a shorter phenotype rather than a severe rice dwarf phenotype[18], this may reflect the functional redundancy of other *ACE1* homologs or compensation by other internode-promoting factors. These results indicate that *ACL1* is expressed in the phase transition in normal paddy rice and, together with GA, controls internode elongation during the reproductive phase. We also revealed *ACE1*-mediated mechanism(s) of internode elongation is conserved in some Gramineae (Extended Data Fig. 10, SI.6). Internodes may shift from the non-elongation to the elongation phase by gaining competency for internode elongation[9,10]. *ACE1* and *ACL1* confer competence to respond to GA at different developmental time points, activating cell division in internode cells, leading to the phase transition from non-elongation to elongation of internodes. Therefore, *ACE1* and *ACL1* represent the regulators proposed by Suetsugu[10] and Inouye *et al*.[11] that determine the initiation of internode elongation.

**DEC1 represses internode elongation**

We previously showed that the *SK1* and *SK2* transcription factor genes on chromosome 12 relating to deepwater response positively regulate total internode length[19](Extended Data Fig. 11a). Positional cloning of the QTL for GA response narrowed down the candidate region to 68 kb, containing four putative genes in T65 and excluding *SK* genes (Fig. 4a, Extended Data Fig. 11b). The 68 kb candidate region with a T65 homozygous or T65/C9285 heterozygous genotype showed suppression of internode elongation in the presence of GA (Extended Data Fig. 11b-d), indicating that the candidate region of

the T65 allele that inhibit internode elongation. Gene expression analysis, CRISPR/Cas9-generated loss-of-function mutant plants, and gene overexpression revealed that *LOC_Os12g42250* is the causal gene in the QTL that functions to repress internode elongation (Fig. 4b-e, Extended Data Fig. 11e-i, SI.7), and we thus named it *DECELERATOR OF INTERNODE ELONGATION1* (*DEC1*). Although several insertions, deletions, and substitutions were detected in the DEC1 amino acid sequence of T65 and C9285, introduction of a *dec1* mutation in T65 and NIL12 (carrying the C9285 allele of *DEC1* in T65) resulted in increased internode elongation (Fig. 4c-e, Extended Data Fig. 11j-l). This genetic analysis suggests that T65 and C9285 *DEC1* alleles are functional and that differences in their expression level, not in their protein functions, affect internode elongation. GA application and DW conditions decreased *DEC1* expression in C9285 but not in T65 (Fig. 4b, f), and so differences in the promoter region would explain the differential expression in the two varieties. In T65 and Nipponbare plants around the transition from vegetative to reproductive phase, *DEC1* showed a gradual decrease in expression while floral meristem identity marker genes, *OsMADS*s, were upregulated (Fig. 4g, Extended Data Fig. 11m). Interestingly, *DEC1* expression was detected in the cell division zone of elongating internodes under SW, but its expression was markedly reduced under DW (Extended Data Fig. 12a). In contrast, cell division marker genes were upregulated at this region under DW (Extended Data Fig.12a). *DEC1* was recently identified as *PINE1*, which is involved in internode elongation during the reproductive phase in Nipponbare[20]. *PINE1* expression decreases during the reproductive phase[20]. These results suggest that de-repression of *DEC1*/*PINE1* by signal(s) derived from developmental maturation, or the phase transition from vegetative to reproductive, promotes the acquisition of internode elongation ability in T65.

*DEC1*/*PINE1* encodes a C2H2 zinc-finger transcription factor with LxLxL-type EAR motifs at the N- and C-termini, and protein was localized in nucleus (Extended Data Figs. 11k, 12b-g). As the EAR

motif is believed to be involved in negative or positive regulation of gene transcription[21,22], we performed a yeast one-hybrid assay to confirm the transcriptional activity of DEC1/PINE1. DEC1/PINE1 did not enhance yeast growth and it suppressed the transcriptional activity of VP16 (Extended Data Fig. 12h, suggesting transcriptional suppression of downstream genes. These results indicate that downregulation of *DEC1*/*PINE1* expression promotes internode elongation by relieving the suppression of expression of downstream genes. The overexpression of *DEC1* in barley also strictly suppressed plant height and internode length (Extended Data Fig. 13a-d), suggesting that the function of *DEC1*/*PINE1* as a suppressor of internode elongation is likely to be conserved in Gramineae.

The *dec1* mutant plants showed internode elongation, which was enhanced by GA treatment (Extended Data Fig. 13e). Two cell division-associated genes (*Histone H4* and *CDKA1*) were expressed constitutively in the internodes of *dec1* both in the absence and presence of exogenous GA (Fig. 4h). In addition, cell division was enhanced in elongating internodes of *dec1*, and GA application further expanded the cell division zone (Extended Data Fig. 13f, g). The results indicate that GA regulates intercalary meristem activity by regulating the function of *DEC1*/*PINE1*. To confirm the relationship among ACE1, DEC1/PINE1 and SKs, we performed expression analysis (Extended Data Fig. 13h-j, SI.8). The results suggest that the internode elongation mechanism controlled by ACE1, DEC1/PINE1 and SKs are independent of each other. Next, we surveyed the natural selection and domestication process of *ACE1* and *DEC1* using wild rice (*O. rufipogon*) and cultivars. Genetic diversity analysis suggests that both *ACE1* and *DEC1* facilitate opposite selection—in domestication and in environmental adaptation—which favored dwarfism and internode elongation, respectively (Fig. 4i, Extended Data Fig. 14a-d, SI.9, Supplementary Table 3, 4). Furthermore, our QTL pyramiding line provides potential application in breeding rice in flooded areas as demonstrated by the yield advantage of combining deepwater rice *ACE1* and *DEC1* alleles (Extended Data Fig. 14e-h, SI.9).

In the past two decades, using mutant plants, we have learned of the role of GA biosynthesis and signaling in regulating plant growth and development[12]. However, the molecular underpinnings of how GA promotes stem elongation has, to date, been elusive. In this study, we identified *ACE1* and *DEC1* as factors that confer the ability to initiate internode elongation in response to GA by using natural diversity, DW rice, thus explaining the concept proposed 50 years ago (Extended Data Fig14i, SI.10). Because *ACE1* and *DEC1*/*PINE1* are conserved and functional in other plant species, such as *Brachypodium* and barley, our findings not only enhance understanding of the regulation of stem elongation in rice but also that of other members of the Gramineae family that may have a similar stem elongation mechanism. Further studies seeking to identify ACE1 interactors and downstream genes of DEC1 using a more diverse panel of rice accessions, including wild rice, will advance our understanding of the regulatory mechanism of the intercalary meristem at internodes. In light of these new discoveries, genetically controlling plant height by targeting factors other than GA biosynthesis or signaling genes is now possible.

## References


1. Kaneko, M. *et al.* Where do gibberellin biosynthesis and gibberellin signaling occur in rice plants? *Plant J.* **35**, 104–115 (2003).
2. Kende, H., Van Knaap, E. Der & Cho, H. T. Deepwater rice: A model plant to study stem elongation. *Plant Physiol.* **118**, 1105–1110 (1998).
3. Sauter, M., Mekhedov, S. L. & Kende, H. Gibberellin promotes histone H1 kinase activity and the expression of *cdc2* and cyclin genes during the induction of rapid growth in deepwater rice internodes. *Plant J.* **7**, 623–632 (1995).
4. Cronk, Q. *The Molecular Organography of Plants*. *Oxford University Press* (2009). doi:10.1093/acprof
5. Sasaki, A. *et al.* A mutant gibberellin-synthesis gene in rice. *Nature* **416**, 701–702 (2002).

6. Peng, J. *et al.* `Green revolution' genes encode mutant gibberellin response modulators. *Nature* **400**, 256–261 (1999).
7. Catling, D. *Rice in Deep Water*. *MacMillan Press* (1992).
8. Kuroha, T. *et al.* Ethylene-gibberellin signaling underlies adaptation of rice to periodic flooding. *Science* **186**, 181–186 (2018).
9. Kawara, H., Chonan, N. & Wada, K. Studies on morphogenesis in rice plants. 3. Interrelation of the growth among leaves, panicle and internodes, and a histological observation on the meristem of culm. *Proceeding Crop Sci. Soc. Japan* **37**, 372–383 (1968).
10. Suetsugu, I. Studies on the first jointing stage in rice plants. *Proceeding Crop Sci. Soc. Japan* **37**, 489–498 (1968).
11. Inouye, J. On floating rice and its ecological traits in Southeast Asia. *Southeast Asian Stud.* **25**, 51–61 (1987).
12. Hedden, P., Thomas, S. G. *Annual Plant Reviews, The Gibberellins. Wiley-Blackwell* (2016).
13. Nagai, K. *et al.* QTL analysis of internode elongation in response to gibberellin in deepwater rice. *AoB Plants* **6**, 1–12 (2014).
14. Hattori, Y. *et al.* A major QTL confers rapid internode elongation in response to water rise in deepwater rice. *Breed. Sci.* **57**, 305–314 (2007).
15. Inouye, J., Kyuragi, T. & Xuan, V.-T. On the growth habits of floating, single- and double-transplanted rice plants in the Mekong Delta. *Japanese J. Trop. Agric.* **22**, 67–70 (1978).
16. Kotogany, E., Dudits, D., Horvath, G. & Ayaydin, F. A rapid and robust assay for detection of S-phase cell cycle progression in plant cells and tissues by using ethynyl deoxyuridine. *Plant Methods* **6**, 1–15 (2010).
17. Kania, T., Russenberger, D., Peng, S., Apel, K. & Melzer, S. *FPF1* promotes flowering in arabidopsis. *Plant Cell* **9**, 1327–1338 (1997).
18. Sakamoto, T. *et al.* An overview of gibberellin metabolism enzyme genes and their related mutants in rice. *Plant Physiology* **134**, 1642-1653 (2004).
19. Hattori, Y. *et al.* The ethylene response factors *SNORKEL1* and *SNORKEL2* allow rice to adapt to deep water. *Nature* **460**, 1026–30 (2009).
20. Gómez-Ariza, J. *et al.* A transcription factor coordinating internode elongation and photoperiodic signals in rice. *Nat. Plants* **5**, 358–362 (2019).
21. Pauwels, L. *et al.* NINJA connects the co-repressor TOPLESS to jasmonate signalling. *Nature* **464**, 788–791 (2010).
22. Li, S. *et al.* Rice zinc finger protein DST enhances grain production through controlling *Gn1a*/*OsCKX2* expression. *Proc. Natl. Acad. Sci. U. S. A.* **110**, 3167–3172 (2013).

## Figure legends

**Figure 1. Internode elongation of normal paddy rice and deepwater (DW) rice.**

**a** and **b**, Gross morphologies of normal paddy rice, T65 (**a**), and DW rice, C9285 (**b**), at each leaf stage (LS) under shallow water (SW) conditions. Leaf stage (LS) is considered an indicator of rice age. T65 matured after 5 to 6 months from seed sowing while C9285 had not yet formed panicles. Arrowheads, panicles. Bars, 1 m. **c**, Total internode length of T65 and C9285 at each growth stage under SW conditions or after 1 week under DW conditions. Data are means ± SD ($n \geq 4$ plants, see Source Data). **d** and **e**, Shoot morphology of T65 (**d**) and C9285 (**e**) in response to various GA concentrations. Treatment of GA, with $10^{-6}$ M uniconazole (an inhibitor of endogenous GA biosynthesis), was performed from seed germination until the 4-week-old seedling stage. Arrowheads indicate the positions of nodes. Bars, 10 cm. **f**, Relative length of the second leaf sheath of plants in **d** and **e.** The length of uniconazole-treated plants was set to 1. Data are means ± SD ($n \geq 5$ plants, see Source Data). **g**, Internode length of T65 and C9285 in **d** and **e** according to GA level. Data are means ± SD ($n \geq 5$ plants, see Source Data). A two-tailed *t*-test was used between C9285 and T65 for each treatment. **h**, Responses of internodes to GA and/or DW. Plants at 6-LS were subjected to the following conditions for 1 week: SW, SW conditions; GA, $10^{-5}$ M $GA_3$ treatment; DW, 1 m water depth; and DW + GA, 1 m water depth and $10^{-5}$ M $GA_3$. 'Initial' indicates the internode length of 6-LS plants before treatment. Data are means ± SD. The number of plants is showed in the panel. One-way ANOVA followed by Tukey's multiple-comparison test. All experiments were repeated three times with similar results.

**Figure 2. ACE1 initiates internode elongation.**

**a**, Temporal responses of the NILs to $10^{-4}$ M $GA_3$ (mean ± SD, n ≥ 6 plants, see Source Data). A two-tailed *t*-test compared with T65. **b.** High-resolution linkage map of *ACE1*. Red arrow, candidate region. Ins and Del, insertion and deletion, respectively. **c**, Gain-of-function analysis of *ACE1*. $T_1$ transgenic plants were treated with $10^{-4}$ M $GA_3$ for 3 weeks after germination. Arrowheads indicate nodes linked by elongated internodes. Bars, 5 cm. **d**, Quantitative data of the total internode length of **(c)**. Data are means ± SD. The number of plants is showed in the panel. One-way ANOVA followed by Tukey's multiple-comparison test. **e**, Overexpressor of *ACE1* in NIL12 ($T_0$) without GA treatment. Right panel is an enlarged view of the boxed area. Bars, 1 cm. Arrowheads, nodes linked by elongated internodes. **f and g**, Quantification of *ACE1* expression with mock and GA treatment **(f)**, and under shallow water (SW) and DW conditions **(g)**. Data are means ± SD (n=4 plants). A two-tailed *t*-test compared with T65 Mock **(f)** or T65 SW **(g)**. **h and i**, Quantification of *ACE1* expression **(h)** and total internode length (cm) under SW and DW conditions at each leaf stage in T65 and C9285 **(i)**. Data are means ± SD. The number of plants is showed in the panel. All experiments were repeated three times with similar results.

**Figure 3. Regulation of gene expression and functional analysis of *ACE1*.**

**a**, Schematic diagram of internode used in histological observations in **b to d**. Immunostaining of ACE1 (red) in C9285 before (**b**) and after GA treatment **(c and d)**. **d**, Enlarged view of the dashed square of **c**. Bars, 1 mm. **e**, Expression of cell division-related genes in the vector control (VC) and $ACE1^{C9285}$ overexpressor in T65 genetic background. RNA was extracted from the seventh internode of 6-leaf stage plants after 3 days of $10^{-4}$ M $GA_3$ treatment (mean ± SD, n = 4 plants). One-way ANOVA followed by Tukey's multiple-comparison test. **f**, Phylogenetic tree of ACE1 homologs in rice. **g**, Quantification of *ACE1* and *ACE1-like1* (*ACL1*) expression at each leaf stage in T65 and C9285 under shallow water (SW) conditions. Rep., reproductive stage. Data are means ± SD (n = 3 plants). A two-tailed *t*-test compared with 5-LS T65 or 5-LS C9285. **h**, Internode length under SW conditions

and after treatment with $10^{-5}$ M $GA_3$. Bars indicate means of plants; colors, each internode lengths. Data are means ± SD. The number of plants is showed in the panel. **i**, Overexpressor of *ACL1* in T65 genetic background. $T_0$ transgenic plants were treated with $10^{-5}$ M $GA_3$ for 3 weeks. Subpanel shows an enlarged view of the basal region of the *ACL1* overexpressor under mock treatment. Arrowheads indicate nodes linked by elongated internodes. Bars, 1 cm. **j**, Quantitative data of the total internode length of **(i).** Data are means ± SD. The number of plants is showed in the panel. **k**, Total internode length of *ACE1*$^{C9285}$ and *ACL1* overexpressors in T65 after ripening. Data are means ± SD. The number of plants is showed in the panel. One-way ANOVA followed by Tukey's multiple-comparison test (**h**, **j** and **k**). All experiments were repeated three times with similar results.

**Figure 4. *DEC1* suppresses internode elongation, and opposite selection of *ACE1* and *DEC1* in domestication and in environmental adaptation.**

**a**, High-resolution linkage analysis of *DEC1*. Red arrow, candidate region. Hatched boxes, deletion of genomic sequences in C9285. **b**, Expression level of *DEC1* before (0 h) or after 24 h of $10^{-4}$ M $GA_3$ treatment. Data are means ± SD (n = 3 plants). A two-tailed *t*-test compared with Mock of T65. **c**, Sequence of the *dec1* mutant generated using the CRISPR/Cas9 system. **d**, Phenotype of the *dec1* mutant without GA treatment. Photographs to the right are enlarged views of the base. Arrowheads indicate nodes linked by elongated internodes. Bars, 5 cm. **e**, Each internode length after ripening. The uppermost internode was defined as the first internode. Data are means ± SD (n = 4 plants). A two-tailed *t*-test compared with control and *dec1*. **f and g**, Quantification of *DEC1* expression under DW conditions **(f)**, and at the indicated leaf stages of T65 **(g)**. Data are means ± SD (n = 4 plants). A two-tailed *t*-test compared with SW of T65 (**f**) or 3-LS (**g**). **h**, Expression of cell division-related genes in the control and *dec1* mutant in T65 genetic background. RNA was extracted from the fifth internode of 5-leaf stage plants after 3 days of $10^{-4}$ M $GA_3$ treatment (mean ± SD, n = 4 plants). One-way

384 ANOVA followed by Tukey's multiple-comparison test. All experiments were repeated three times
385 with similar results. **i**, Model for evolutionary paths of *ACE1* and *DEC1* showing divergence of wild
386 and domesticated rice.

## Methods

### Plant materials and growth conditions

The *japonica* cultivar T65 (*Oryza sativa* cv. Taichung 65) was maintained at Nagoya University, Nagoya, Japan. C9285 (*O. sativa* var. C9285 syn. Dowai38/9) was provided by the National Institute of Genetics of Japan. The rice seeds were sterilized at 60°C for 10 min, germinated in water (30°C for 3 days), sown in perforated plastic pots (9 × 9 × 12 cm) filled with soil (N, P, and K at 0.25, 0.3, and 0.25 g/kg, respectively; Medel Ltd.), and grown in a greenhouse under natural light conditions at Nagoya University. The water level in the pots was maintained at ~5 cm above the soil surface (SW condition). For the DW treatment, plants were placed in a 120-cm-tall tank and completely submerged in water (DW conditions) for phenotypic evaluation. For GA (Gibberellin $A_3$ Standard; CAS RN: 77-06-5; Wako) treatment, seeds were sown individually in a perforated cell tray (cell size, 2.5 × 2.5 × 4.5 cm). To eliminate the effect of endogenous GA, uniconazole (uni; Uniconazole P Standard; CAS RN: 83657-17-4; Wako), an inhibitor of GA biosynthesis, was administered with or without GA from germination. For the GA and uni treatment, 2 mL or 200 µL of a $10^{-1}$ M $GA_3$ stock solution in ethanol and 0.2 mL of a $10^{-2}$ M uni stock solution were added to 2 L of water (final concentration, $10^{-4}$ M for seedlings and $T_1$ transgenic plants or $10^{-5}$ M GA for $T_0$ transgenic plants, and $10^{-6}$ M uni). For the mock treatment, 2 mL of ethanol was added to 2 L of water. Each solution was used to treat 140 individuals. Seedlings were grown under 16 h of light and 8 h of darkness with 70% humidity at 25°C in a phytotron. After 1 to 4 weeks, measurements were conducted.

### Quantification of hormone levels

Plants were grown until the 5- or 8-leaf stage under SW conditions. After submergence for 24 h, the region from 0 to 1 cm above the uppermost node, including elongating internodes, was harvested and

frozen in liquid nitrogen. Gibberellins and ABA were quantified using an ultra-high performance-liquid chromatography (UHPLC)-electrospray ionization (ESI) quadrupole-orbitrap mass spectrometer (UHPLC/Q-Exactive™; Thermo Scientific) as described previously[23,24] with an ODS column (AQUITY UPLC HSS T3, 1.8 mm, 2.1 x 100 mm; Waters).

**Immunoblot analysis**

To determine the endogenous SLR1 level, a stem section including elongating internodes was sampled from the 6-LS of T65 and C9285 after $10^{-4}$ M $GA_3$ treatment for the indicated times (Extended Data Fig. 2i). Gel electrophoresis and immunodetection were performed according to the method of Minami *et al*.[25] with some modifications. Total proteins were extracted using total protein extraction buffer (50 mM Tris-HCl [pH 8], 150 mM NaCl, 0.5 % (v/v) Triton X-100, 5 mM EDTA, 1 mM DTT, 1 mM PMSF, and 1× complete protease inhibitor cocktail). Protein concentration was measured using Protein Assay Dye Reagent Concentrate (BioRad). Equal amounts of extract were subjected to gel electrophoresis, and proteins were transferred to a polyvinylidene difluoride membrane (Immobilon) using a Trans-Blot Turbo (Bio-Rad). The primary rabbit anti-SLR1 antibody, validated by Ueguchi-Tanaka *et al*.[26], for providing was used at a 1/2,000 (v/v) dilution in TBS-T with skim milk. After the goat anti-rabbit IgG-HRP secondary antibody (Invitrogen) reaction (1/10,000 dilution), proteins were detected using the SuperSignal West Dura Extended Duration Substrate (ThermoFisher). Signals were detected by Light-Capture II (ATTO). An antibody against $ACE1^{C9285}$ was prepared by immunizing rabbits with the synthetic peptide NH2-C+ VLKNRDHFKVLDN-COOH (positions 96–108 of $ACE1^{C9285}$). Peptide synthesis and antibody purification were performed by Eurofins Genomics. For production of $ACE1^{C9285}$ protein fused with glutathione S-transferase (GST), cDNA sequence of $ACE1^{C9285}$ was amplified using specific primers (Supplementary Table 5), and cloned into an expression vector, pGEX-4T-1 (GE Healthcare). The *E. coli* Rosetta (DE3) pLysS (Novagen) was

used for the protein expression. The bacterial culture (3 mL) was grown overnight and further inoculated into the LB medium (100 mL) containing 50 g/mL ampicillin. After the culture reached the $OD_{600}$ of 0.5 - 0.7, isopropyl-1-thio-β-d-galactopyranoside (IPTG) was added at 1 mM concentration and incubated at 22°C for 18 h. The cells were collected by centrifugation, and then suspended and sonicated in the lysis buffer [100 mM NaCl, 10 mM Tris-HCl, 0.5 mM dithiothreitol (DTT), and 1x Complete protease inhibitor cocktail (Roche)]. After electrophoresis, proteins were transferred to a polyvinylidene difluoride membrane (Immobilon) using a Trans-Blot Turbo (Bio-Rad). The primary rabbit anti-ACE1 antibody was used at a 1/1,000 (v/v) dilution in TBS-T with skim milk. After the goat anti-rabbit IgG-HRP secondary antibody (Invitrogen) reaction (1/10,000 dilution), proteins were detected using the SuperSignal West Dura Extended Duration Substrate (ThermoFisher). Signals were detected by Light-Capture II (ATTO).

**Positional cloning**

NIL3, NIL12, and NIL3+12, which have C9285 segments for the DW response QTLs on chromosomes 3, 12, and 3/12, respectively, in T65 genetic background were described previously[19]. The markers used for genotyping of NILs are listed in Supplementary Table 5. Positional cloning by linkage analysis was performed using a mapping population from a cross between NIL3+12 and NIL12 for QTLs on chromosome 3 (Extended Data Fig. 3h) and NIL3+12 and NIL3 for QTLs on chromosome 12. $F_2$ plants showing recombination between the markers RM7249 and 9k were selected. The $F_3$ recombinant plants were selfed and used for high-resolution linkage analysis. Bacterial artificial chromosome (BAC) clones of C9285 and T65, C9285_32A02, and T65_GN26L06 of chromosome 3 and C9285_10H05 of chromosome 12, covering the candidate regions were selected from the library. For phenotypic evaluation, the total internode length after GA treatment for 4 weeks was measured.

**Construction of the BAC library and sequencing of BAC clones**

Megabase-sized rice DNA was isolated from young leaves of T65 and C9285 using a method described previously[27]. A BAC library was created as follows: DNA was digested by *Hin*dIII, high-molecular-weight DNA was fractionated according to size by pulsed-field gel electrophoresis (CHFF; Bio-Rad Laboratories, Hercules, CA, USA), ligated into a vector (pIndigo BAC-5; Epicentre Bio-Technologies, Madison, WI, USA), and transformed into *Escherichia coli* DH10B. The BAC library, which contained 21,546 clones with an average insert size of 135 kb, was screened by PCR using tightly linked DNA markers. Positive BAC clones completely covering the gene region were subjected to capillary sequencing (ABI3730; Applied Biosystems, Foster, CA, USA) using a shotgun strategy as described previously[28].

**Production of transgenic plants**

For gain-of-function analysis of *ACE1*, 7.7-kb genomic DNA fragments of C9285 (Fig. 2c) and T65 containing the entire coding region of *ACE1*, 5.2 kb of the upstream region, and 2.2 kb of the downstream region were amplified from the BAC clones, C9285_32A02 and GN26L06, by PCR using KOD Fx Neo (Toyobo, Japan). The fragment was fused to the binary plant transformation vector pCAMBIA1300. For overexpression of *ACE1*, *DEC1*, and *SUB1C*, cDNA fragments were amplified and fused to pCAMBIA1380 harboring the maize (*Zea mays*) *UBIQUITIN1* promoter. The *dec1* mutants were generated using the CRISPR/Cas9 system according to Mikami *et al.*[29]. The primers used are listed in Supplementary Table 5. The resulting constructs were introduced into the T65, NIL3, or NIL12 background by *Agrobacterium tumefaciens* (EHA105)-mediated transformation according to Hiei *et al.*[30].

**Analysis of gene expression**

Total RNA was extracted using a Maxwell RSC Instrument (Promega, Madison, WI, USA) according to the manufacturer's protocol. First-strand cDNA was synthesized with the Omniscript RT Kit (Qiagen, Hilden, Germany) and oligodT20 primers. Quantitative RT-PCR (qPCR) was performed using the StepOne™ Real-Time PCR System (Applied Biosystems) with Thunderbird SYBR qPCR Mix (Toyobo). Expression levels were normalized to that of rice *ubiquitin*. Plasmid DNA containing the cDNAs were used as templates to generate standard calibration curves. The primers used for qPCR are listed in Supplementary Table 5.

**Systematic identification of trans-eQTL regulating *ACE1* expression**

To evaluate the molecular and genetic basis of DW response in DW rice, we previously carried out an expression quantitative trait loci (eQTL) analysis of recombinant inbred line populations of non-DW (Taichung 65) and DW rice (Bhadua)[31]. To identify *trans*-eQTLs of ACE1 using the dataset of Kuroha *et al*.[31], we conducted genome-wide eQTL mapping using the R/qtl[32] and R/eqtl packages[33]. We used a support interval of 1.5 and the default settings in the R/eqtl::define.peak() function to evaluate QTLs and support intervals.

**Analysis of transactivation**

cDNA fragments of *bZIP71* (*Os09g0306400*), *SUB1B* (*Os09g0287000*), and *SUB1C* (*Os09g0286600*) were amplified by PCR using gene-specific primers (Supplementary Table 5) and fused to pUC19 harboring the maize (*Zea mays*) *UBIQUITIN1* promoter. The p*Ubi*:*Luc* harboring the *Luciferase* gene fused with the maize *UBIQUITIN1* promoter was used as an internal control plasmid. The control reporter plasmid was pUC19 harboring the luciferase reporter gene *hRluc* (*Renilla reniformis*). The reporter plasmids, *pACE1*:*hRluc*, were constructed by introducing DNA fragments corresponding to the promoter regions of *ACE1* from before the start codon of ACE1 (−1 bp) to −4741 bp of T65 or

−4404 bp of C9285 (Extended Data Fig. 6c) into pUC19, respectively. For transfection, plasmids were purified from *E. coli* cultures using a Plasmid Maxi Kit (Qiagen) and adjusted to 2 μg/μL. Transactivation analysis was performed by bombardment (IDERA/GIE-III; Tanaka Co., Ltd., Sapporo, Japan) of 1.0μ m gold particles (Bio-Rad) coated with plasmid into the aleurone layer of rice seeds. Rice seeds were prepared by removing the embryos, cutting them vertically, and immersing each half in buffer (20 mM succinic acid, 20 mM calcium chloride) for 24 h. Subsequently, the seed coat was peeled and subjected to particle bombardment. The gold particles were absorbed with p*Ubi*:*Luc*, an effector plasmid, and a reporter plasmid. After bombardment for 24 h, seeds were ground in extraction buffer (100 mM potassium phosphate, 2 mM dithiothreitol, 2 mM ethylenediaminetetraacetic acid [EDTA], and 5% glycerol) and the supernatant after centrifugation was employed for LUC (BrillianStar-LT; Toyo Ink) and hRluc (Renilla Luciferase Assay System; Promega) assays using Lumat LB 9507 (Berthold Technologies, Bad Wildbad, Germany).

**Subcellular localization**

cDNA fragments of *SUB1C* (*Os09g0286600*), $ACE1^{T65}$, $ACE1^{C9285}$, $DEC1^{T65}$ and $DEC1^{C9285}$ were amplified by PCR using gene-specific primers (Supplementary Table 5) and introduced in 35S: GFP/ pUC19. Four μg each of 35S:GFP, 35S:*SUB1C*-GFP, 35S:$ACE1^{T65}$-GFP, 35S:$ACE1^{C9285}$-GFP, 35S:$DEC1^{T65}$-GFP, 35S:$DEC1^{C9285}$-GFP plasmids were coated on 1 mg gold micro carrier (Bio-rad) in buffer (1 M $CaCl_2$, 15 mM spermidine). Four μg of 35S:mCherry plasmid was added to each mixture as control and mixed vigorously using a vortex for 2 min. Plasmid-coated micro carrier was dehydrated with 100 % ethanol prior to bombardment. The inner layer of onion was cut into 2 cm x 3 cm and placed in a petri dish with filter paper containing sterile water. Bombardment is performed according to the standard procedure of PDS-1000/He provided by the manufacturer (Bio-rad). Micro carrier was accelerated with a helium burst at 1350 psi. Petri dishes were wrapped in foil and kept in the dark

overnight at room temperature. Photographs were taken using a confocal laser scanning microscope (LSM700; Carl Zeiss, Oberkochen, Germany). Fluorescence profiles were imaged by the profile tool of the ZEN software (Carl Zeiss, Oberkochen, Germany).

**Immunohistological staining**

ACE1$^{C9285}$ immunostaining of elongating internodes was performed using the antibody against ACE1$^{C9285}$ (1/1,000 dilution) and secondary antibody, Alexa Fluor 555 goat anti-rabbit IgG (Invitrogen) (1/3,000 dilution) according to Yamaji and Ma[34]. Sections 100-mm thick were visualized by confocal laser scanning microscopy (LSM700; Carl Zeiss, Oberkochen, Germany).

**Detection of cell division**

To identify dividing cells, we performed an EdU assay. EdU is incorporated into DNA during its synthesis (i.e., during S-phase)[16]. A dissected shoot apex containing elongating internodes was incubated and rotated in water containing 10 μM EdU (Click-iT EdU Alexa Fluor 488 imaging kit; Invitrogen). After 24 h, the samples were fixed in 5% formaldehyde in PBS (pH 7.4) for 2 h and washed three times in PBS. Coupling of EdU to the Alexa Fluor substrate was performed in the dark in the Click-iT reaction mixture, according to the manufacturer's instructions. Photographs were taken using a confocal laser scanning microscope (LSM700; Carl Zeiss, Oberkochen, Germany).

**Transactivation activity assay in yeast**

The full-length cDNA of DEC1 and VP16 was amplified by PCR and fused to the GAL4-DNA binding domain (BD) in pGBKT7 (Clontech, TaKaRa Bio USA, Inc.). The resulting plasmids (pGBKT7-DEC1$^{T65}$, pGBKT7-DEC1$^{C9285}$, pGBKT7-VP16, pGBKT7- VP16-DEC1$^{T65}$, and pGBKT7- VP16-DEC1$^{C9285}$) were transformed into the yeast strain AH109 (Takara bio). The yeast liquid cultures were

serially diluted to an absorbance at 600 nm of 0.6, and 2 μL of each dilution were inoculated onto tryptophan- and histidine-negative synthetic dropout medium.

**_Brachypodium_ growth conditions**

Mature seeds of *Brachypodium distachyon* (L.) P. Beauv. (purple false brome), line Bd21 (USDA National Plant Germplasm System), were placed on two layers of damp sterile filter paper in sterile Petri dishes. The dishes were kept for 2–3 days in the dark at 4°C to synchronize germination and subsequently transferred to 25°C (16 h photoperiod) for 5 days. Germinated seedlings were transplanted to pots filled with sterile soil. Plants were placed on cultivation racks and grown at 22°C under a 20 h photoperiod.

**Transformation in _Brachypodium_**

Plasmids constructed for rice transformation were also used for *Brachypodium* transformation. Embryogenic calli were induced from immature embryos for the production of transformation target tissue as described by Himuro *et al.*[35]. *Agrobacterium tumefaciens* EHA105 was used for transformation. The infection of embryogenic calli with *Agrobacterium* was performed as described previously[36] with modifications. Infected calli were incubated for 2 days at 27°C in the dark. After co-cultivation, the calli were subcultured twice for 14 days on embryogenic callus induction medium (CIM) containing 40 mg/L hygromycin. After 4 weeks of subculture under selective conditions, hygromycin-resistant calli were transferred to regeneration medium (CIM removed 2,4-D) containing 0.2 mg/L kinetin for 2-4 weeks at 25°C in the light for shoot formation. All regenerated shoots were transferred to hormone-free 40% MS medium. After approximately 4 weeks, rooted plants were transferred to soil and analyzed by PCR to confirm the presence of the *hygromycin phosphotransferase* (*hpt*) transgene. Genomic DNA was isolated from leaf tissue of transgenic plants ($T_0$) using the Automatic Genomic DNA Isolation System PI-200 (Kurabo Co. Ltd., Osaka, Japan).

**Trait investigation of transgenic *Brachypodium***

After transplanting in soil and acclimation for 4 weeks, the transgenic lines overexpressing *ACE1* were measured for internode length. *ACE1* knock-down transgenic lines were treated with $10^{-4}$ M $GA_3$ to confirm internode elongation after 3 weeks of acclimation. After 2 weeks, the internode length in knock-down transgenic lines was compared with that of vector control plants.

**Transformation in barley**

To generate transgenic barley (*Hordeum vulgare*), the *Agrobacterium*-mediated transformation method was employed as described previously[37]. Briefly, cv. Golden Promise was grown under a 12 h daylight photoperiod for 2 months then under a 16 h daylight photoperiod with 15°C (day)/13°C (night) in a growth chamber for collecting immature embryos. The immature embryos were infected and co-cultivated with *Agrobacterium tumefaciens* AGL1 carrying p*Ubi*:*ACE1*$^{C9285}$/pCAMBIA1380, p*Ubi*:*DEC1*$^{T65}$/pCAMBIA1380, or p*Ubi*:*DEC1*$^{C9285}$/pCAMBIA1380 for 3 days. Next they were incubated on callus induction medium for 1 week and transferred to selection medium containing hygromycin in the dark at 25°C for 4 weeks. Hygromycin-resistant calli were transferred onto regeneration medium and incubated under a 16 h daylight photoperiod at 25°C. Regenerated shoots were transferred into rooting medium. To confirm the presence of transgenes, DNA was isolated from the regenerated plants using the Kaneka Easy DNA Extraction Kit version 2 (Kaneka Co., Japan), and touch-down PCR[37] was performed using specific primers for *HPT* (hph1; 5'-GCTGGGGCGTCGGTTTCCACTATCGG-3' and hph2; 5'-CGCATAACAGCGGTCATTGACTGGAGC-3'), *ACE1* (62_22510_XbaI_F; 5'-AGCTCTAGAATGGCGGGGACGGGGGTGTG-3' and 64_22510_(C9)_SmaI_R; 5'-CATCCCGGGCTAGTTATCGAGGACCTTGA-3') and *DEC1* (351_SK4_HindIII_F; 5'-ACTAAGCTTATGGAGGCTCCCCCTTCTCT-3' and 352_SK4_SpeI_R; 5'-

GGCACTAGTCTAGAGCTTCAGGTTGAGAT-3') genes. The regenerated plants with transgenes were transplanted into the soil and grown under 16 h of daylight at 15°C (day)/13°C (night) in a growth chamber. The phenotype of transgenic plants was evaluated 5 weeks after transplanting.

**Transformation in sugarcane**

Calli of the Japanese commercial sugarcane cultivar KRFo93-1 were induced according to previous report[38] and were used as target tissue for particle bombardment using a PDS-1000/He helium-driven biolistic device (Bio-Rad). The basic bombardment parameters were the same as those employed for genetic transformation of Italian ryegrass[39].

The calli were co-bombarded with the plasmids pAcH1[40] and p*Act:ACE1*$^{C9285}$/pCAMBIA1380. The plasmid pAcH1 harbors the *hygromycin phosphotransferase* (*hpt*) gene, and the plasmid p*Act:ACE1*$^{C9285}$/pCAMBIA1380 harbors the *ACE1* gene. The plasmid p*Act*/pCAMBIA1380 was also co-bombarded with pAcH1 as a vector control.

The bombarded calli were incubated for 2 days in the dark at 25°C, transferred to selection medium (CIM with 150 mg/L hygromycin), and subcultured on fresh selection medium every 2 weeks. Hygromycin-resistant calli that appeared during selection culture were isolated and cultured on phytohormone-free regeneration medium (RM) containing 3 g/L activated charcoal and MS vitamins under continuous fluorescent light (40 μmol/m$^2$/s) at 25°C until green shoots, regenerated from resistant calli, and rooting occurred. The rooted plants were established in soil and grown in a glasshouse at 28°C.Transformation of the regenerated plants was confirmed by PCR using Ampdirect Plus (Shimazu, Kyoto, Japan) according to the manufacturer's instructions. The primer sets used were 5′-CGCATAACAGCGGTCATTGACTGGAGC-3′ and 5′-GCTGGGGCGTCGGTTTCCACTATCGG-3′ to detect the 375-bp fragment of the HPT gene in the pAcH1, and 5′-GGAGAGGACACGCTGAAATC-3′ and 5′-GAGACGCTGTCGAACTTTTC-3′ to

612 detect the 151-bp fragment of p*Act*/pCAMBIA1380, and p*Act:ACE1*$^{C9285}$/pCAMBIA1380. Reactions
613 to detect these fragments were carried out in a ProFlex™ PCR System (Thermo Fisher Scientific,
614 Waltham, MA, USA) with denaturation at 94°C for 30 s, annealing at 60°C for 1 min, and extension
615 at 72°C for 30 s. The amplified fragments were pre-stained with GelRed™ (Biotium, Inc., Fremont,
616 CA, USA), electrophoresed with Mupid-exU (Mupid, Tokyo, Japan) in 1.5% (w/v) agarose gels at
617 70 V for 30 min in Tris-borate EDTA buffer, and photographed using a Mupid-Scope WD
618 transilluminator (Mupid, Tokyo, Japan).

619 **Genetic diversity and indices of selective sweeps surrounding *ACE1* and *DEC1***

620 The fastq files of 28 *O. rufipogon*, registered in OryzaGenome (from "Deep Sequenced Accessions
621 List"; http://viewer.shigen.info/oryzagenome2detail/index.xhtml), were mapped to the Nipponbare
622 reference genome (Os-Nipponbare-Reference-IRGSP-1) using BWA (bwa-mem)[41] using the default
623 value for mismatch allowance. The VCF format files were created from the bam files using only
624 uniquely mapped reads, to call genome-wide binary polymorphisms. For *DEC1*, a short insertion in
625 the promoter region of the mutated (inactive) allele (unpublished results), which form a conserved
626 haplotype with the surrounding polymorphisms in the *O. rufipogon* population, was defined as the
627 core polymorphism representing the mutated allele in the following extended haplotype
628 homozygosity (EHH)-based detection of selective sweeps. To infer the contribution of *ACE1* and
629 *DEC1* mutations to internode elongation under DW conditions, a multiple regression test was
630 conducted with the generalized linear model (GLM) in R, using the genotypes in these two loci.
631 Estimation of haploblocks, or phasing, was performed with Beagle 5.0[42], using the VCF files
632 described above for *O. rufipogon*, and from the "3K RG 29mio biallelic SNPs" dataset registered in
633 the 3K RGP and Oryza SNPs project (IRRI, http://snp-seek.irri.org/download.zul) for *O. sativa*.
634 Individuals of six *O. sativa* subpopulations (japonica-temperate, -subtropical, and –tropical, and

635 indica-1, -2, and -3) were selected based on their genome structures, which have not undergone
636 substantial introgressions with the other subpopulations. Alleles, the frequency of which was less
637 than 3% or the miss rate was over 0.5, were pruned before phasing. Phased VCF files per
638 (sub)populations were subjected to selscan[43] to determine Pi values, allele frequencies, extended
639 haplotype homozygosity (EHH)[44], and integrated haplotype score (iHS)[45]. The unstandardized iHS
640 output from selscan was normalized to the genome-wide iHS values to calculate the p-value of each
641 core polymorphism.

642 **Statistics and reproducibility**

643 Prism 7 software was used to evaluate significant variations using a two-tailed t-test or one-way
644 ANOVA. Tukey's multiple-comparison test were used to assess the statistical difference in
645 comparisons after a one-way ANOVA. The *P* values calculated are shown in each graph above the
646 line that connects the two sets of data. For all Figures or Figure legends, n represents the number of
647 independent biological replicates.

648 **The data availability statement**

649 The gene sequences used in this work have been deposited at DDBJ
650 (https://www.ddbj.nig.ac.jp/index-e.html; *ACE1*$^{C9285}$: LC543529; *ACE1*$^{short}$: LC543530; and
651 *DEC1*$^{C9285}$: LC543531). The datasets of RNA-sequencing analyzed during the current study are
652 available in the Minami *et al*. (http://www.plantphysiol.org/content/176/4/3081/tab-Figures-data)[27].
653 Microarray data for trans-eQTL analysis are available in the NCBI GEO database (accession no.
654 GSE87702). The fastq files of *O. rufipogon* are available in OryzaGenome (from "Deep Sequenced
655 Accessions List"; http://viewer.shigen.info/oryzagenome2detail/index.xhtml). 3K RG 29mio biallelic
656 SNPs dataset registered in the 3K RGP and Oryza SNPs project (IRRI, http://snp-

seek.irri.org/download.zul). Source Data for Figs. 1–4 and Extended Data Figs.2-6, 8-14 are provided with the paper.

**Extended Data**

**Extended Data Figure 1. Schematic diagram of a rice plant and the concept of timing of internode elongation.**

**a to c**, Measurement and concept of initiation of internode elongation. The growth stage of rice plant is defined by the number of fully expanded leaves. For example, the right plant in **a** is at the 6-leaf stage. Plant height and total internode length were defined as the length from the base to the leaf top and from the base to the end of the uppermost internode, respectively. **a**, Schematic diagram of rice showing no internode elongation during the vegetative phase. **b**, Schematic diagram of rice showing internode elongation at the 6-leaf stage. **c**, Schematic diagram of rice showing internode elongation at the 3-leaf stage. It has been reported that the lowest elongated internode (LEI), proposed as an index of initiation of internode elongation, is correlated with the total internode length and number of elongated internodes. In **a**, LEI was not determined because the plant did not elongate internodes. In contrast, the LEI was 6 and 3 because internode elongation started from the 6- and 3-leaf stages in **b** and **c**, respectively. Initiation of internode elongation is influenced by activation of the intercalary meristem in internodes[3] and comparison of LEI reveals the timing of the acquisition of internode elongation ability. However, the factors that directly control this trait have not yet been identified.

**Extended Data Figure 2. Changes in shoot phenotype under shallow water (SW) and deepwater (DW) conditions.**

**a**, The plant height of T65 and C9285 was measured at each leaf stage under SW conditions. Data are means ± SD (n ≥ 3 plants, see Source Data). **b**, Expression level of *OsMADS14* (*OsAP1B*: *LOC_Os03g54160*) and *OsMADS15* (*OsAP1A*: *LOC_Os07g01820*) at each growth stage of T65 (n = 3 plants) and C9285 (left panel: n = 3 plants; right panel: n = 4 plants). Data are means ± SD. One-way ANOVA followed by Tukey's multiple-comparison test. *OsMADS14* and *OsMADS15* are activated during the growth phase transition from the shoot apical meristem to the inflorescence meristem by Hd3a (rice FT), OsFD1, and 14-3-3 protein complex[46-49]. Therefore, *OsMADS14* and *OsMADS15* were used as phase transition markers. RNA was extracted from shoot apices at the 5-, 7- and 12-leaf stages containing shoot apical meristem, base of young leaves, immature internodes, and nodes. *OsMADS14* and *OsMADS15* expression was low at the 7-leaf stage but their expression drastically increased at the 12-leaf stage in T65, suggesting that the phase transition occurred at this stage under natural conditions. Internode elongation started after phase transition (T65 elongated internodes after the 11-leaf stage [Fig. 1c]). In contrast, C9285 did not express *OsMADS14* and *OsMADS15* at these leaf stages. Right panels, expression level of *OsMADS14* and *OsMADS15* in 1- and 7-month plants of DW rice C9285. C9285 showed expression of *OsMADS14* and *OsMADS15* 3 months later than normal paddy rice. This suggests that C9285 elongates internodes without a phase transition (Fig. 1c). **c to e**, Plant height **(c)**, total internode length **(d),** and number of elongated internodes **(e)** after seed maturation. Data are means ± SD (n = 5 plants). Numbers indicate *P* value derived from a two-tailed *t*-test. T65 required 6 months from germination until seed maturation whereas C9285 needed 9 months in our condition. Numbers above bars indicate significant differences by Student's *t*-test. **f**, Hormone contents during plant growth under shallow water (SW) and deepwater (DW) conditions. $GA_1$, $GA_4$, abscisic acid (ABA), and indoleacetic acid (IAA) contents at the 5-leaf stage (upper) and 8-leaf stage (lower) of T65 and C9285 under SW and DW conditions. Data are means

± SD (n = 3 plants). One-way ANOVA followed by Tukey's multiple-comparison test. **g**, Temporal responses of internode length to $10^{-4}$ M $GA_3$. GA treatment was started from germination and internode length was measured weekly. Data are means ± SD (n = 6 plants). Numbers indicate *P* values derived from a two-tailed *t*-test compared with C9285 and T65 for each point. **h**, Internode length of T65 and C9285 according to GA concentration in Fig. 1g. Right panel shows an enlarged view, from 0 to 2 cm, of the left panel. Colors show internode lengths. Data are means ± SD. The number of plants is showed in the panel. **i**, SLENDER RICE1 (SLR1) degradation under GA treatment. Western blotting of degradation of SLR1 after GA treatment using a rabbit anti-SLR1 antibody. SLR1, a DELLA protein of rice and master growth repressor in GA signaling, is degraded by the 26S proteasome via the GA-dependent $SCF^{GID1}$ complex, resulting in derepression of GA responses[50,51]. GA treatment was performed on 6-LS plants of T65 and C9285, and total proteins of the stem section were extracted. Arrow indicates the position of SLR1. Ponceau-S, loading control. GA-dependent degradation of SLR1 was observed in the internode of T65, which showed no internode elongation by GA, as in C9285. All experiments except hormone quantification (one time) were repeated two times with similar results.

**Extended Data Figure 3. Internode elongation with growth phase and quantitative trait locus (QTL) related to GA and the deepwater (DW) response.**

**a**, Normal paddy rice does not elongate internodes during the vegetative phase, but it elongates internodes immediately after the reproductive phase (attributed to promotion of GA biosynthesis) under shallow water (SW) conditions. Under DW conditions, internodes do not elongate during the vegetative phase[8,14]. Therefore, the plant cannot survive due to oxygen deprivation under DW conditions. **b**, DW rice shows vigorous growth and an increased plant height due to internode

elongation even under SW conditions (Fig. 1c and Extended Data Fig. 2). Furthermore, when DW rice is exposed to DW conditions, it exhibits rapid internode elongation due to GA accumulation, resulting in exposure of leaves on the water, thus avoiding oxygen deficiency[8]. **c**, Regulation of plant hormone crosstalk induced by DW during the vegetative phase. The DW condition induces ethylene accumulation in the plant body in DW rice and normal paddy rice, which reduces the level of abscisic acid (ABA), an antagonist of GA[19,52,53]. Accumulated ethylene also increases the expression level of *GA20ox2*, which is involved in GA biosynthesis, in DW rice. However, accumulated ethylene does not stimulate *GA20ox2* expression in T65[8]. Therefore, internode elongation by GA is induced in DW rice but not in normal paddy rice. **d**, QTL analysis of GA-responsive internode elongation using recombinant inbred lines of normal paddy rice (T65) and DW rice (Bhadua) detected five QTLs on chromosome 3, 8, 9, 10, and 12 (red)[13]. QTLs for total internode length (TIL) under DW conditions were detected on chromosomes 1 and 12 (blue)[14]. The positions of QTLs are shown with reference to the physical distance of the markers in the QTL analyses. The gene responsible for the QTL on chromosome 1 was *GA20ox2*, which encodes a GA-synthesis enzyme[8]. We also identified two ethylene-related transcription factor genes, *SK1* and *SK2*, as responsible for the QTLs of TIL on chromosome 12[19]. The QTL regulating the lowest elongated internode (LEI) that regulates the timing of initiation of internode elongation under DW conditions was detected on chromosomes 3 and 12 (orange)[14,54-56]. The QTLs for GA response on chromosomes 3 and 12 and the LEI for the DW response overlapped. Therefore, the same genes may be responsible for these QTLs. **e**, Genotypes of near-isogenic lines (NILs). Red and blue, C9285 and T65 genomic regions, respectively. NIL3 and NIL12 possess the quantitative trait locus (QTL) regions on chromosomes 3 and 12 for the initiation of internode elongation in response to gibberellic acid (GA) and deepwater (DW) conditions, respectively, in T65 genetic background. NIL3+12 possesses both QTLs. **f and g**, Total internode length of T65,

NIL1, NIL3+12, and NIL1+3+12 under exogenous GA treatment or DW conditions. **f,** Total internode length under mock and exogenous GA treatment for 3 weeks from germination. Number indicates *P* value derived from a two-tailed *t*-test (means ± SD, n =9 plants). **g**, Total internode length of 8-LS plants under SW and DW conditions for 1 week. Number indicates *P* value derived from a two-tailed *t*-test (means ± SD, n =4 plants). **h**, Mapping of quantitative trait loci (QTLs) on chromosome 3. NIL3+12 and NIL12 were used as the parental lines (P). Red and blue, C9285 and T65 genomic regions, respectively. NIL3+12 possesses QTLs on chromosomes 3 and 12 while NIL12 possesses a QTL on chromosome 12. The $F_1$ population derived from crossing of parental lines resulted in a heterozygous genotype on chromosome 3 and a C9285 homozygous genotype on chromosome 12. By selfing of $F_1$, an $F_2$ recombinant population with segregating genotypes on chromosome 3 was produced. $F_2$ plants showing recombination between the two markers (RM7249 and 9k were used for initial screening) were selected (red dotted rectangles). The $F_3$ population was produced by selfing of the $F_2$ plants. The $F_3$ population was expected to be segregated into three genotypes: homozygous with recombination, heterozygous, and homozygous with no recombination in a 1:2:1 ratio. Homozygotes were selected and used for high-resolution linkage analysis with GA treatment for 3 weeks after germination. For positional cloning of QTL on chromosome 12, the mapping population derived from the cross between NIL3+12 and NIL3 was used, and subsequent genotyping was performed using DNA markers on chromosome 12 (Extended Data Table 5). **i and j**, Dominant effect of the quantitative trait locus (QTL) on chromosome 3 on the response to GA. **i**, Genotype of $F_1$ derived from the cross between NIL3+12 and NIL12. Only chromosome 3 showed a heterozygous genotype and segregated in $F_2$ progeny. **j**, The segregating genotype (left) and internode length (right). Data are means ± SD. The number of plants is showed in the panel. One-way ANOVA followed by Tukey's multiple-comparison test. The progenies of #59 and #58 plants segregated as C9285-type homozygote, T65-type homozygote, and

heterozygote at the region of RM7249 to 9k. Heterozygous plants showed similar internode length to C9285-type homozygotes, suggesting that the C9285-type QTL on chromosome 3 exerts the dominant effect on the GA response of internodes. **k**, Comparison of internode elongation in response to GA and DW conditions. Left panel, genotype of the GA-mapping lines. Middle panel, internode length of the mapping lines with GA treatment for 3 weeks. Right panel, internode length of mapping lines under DW conditions for 1 week. Data are means ± SD. The number of plants is showed in the panel. Number indicates *P* value derived from a two-tailed *t*-test. **l**, Internode length of T65 and NIL3 under shallow water (SW) or DW conditions using 8-leaf-stage plants. DW conditions were maintained for 1 week. Data are means ± SD. The number of plants is showed in the panel. One-way ANOVA followed by Tukey's multiple-comparison test. The data suggest the QTL on chromosome 3 that regulates initiation of internode elongation (lowest elongated internode [LEI] for the DW response) corresponds to the GA-responsive QTL. All experiments were repeated two times with similar results.

**Extended Data Figure 4. The role of *ACE1*.**

**a**, Coding sequence of *ACE1*. The *ACE1* in T65 is 321 bp in size and that of C9285 is 327 bp. *ACE1* of T65 has an additional guanine (G) and one single-nucleotide polymorphism at the end of the coding sequence. **b**, Alignment of the amino acid sequences of ACE1. Nuclear localization signal (NLS) was predicted in $ACE1^{T65}$, but not in $ACE1^{C9285}$ by WOLF PSORT (https://www.genscript.com/wolf-psort.html) **c**, Structure of *ACE1*. The short *ACE1* transcript in T65 and C9285 is 207 bp. Gray and blue boxes, non-coding and coding sequences, respectively. Hatched box, region encoding different amino acids compared with other sequences. The allele for the long *ACE1* transcript in T65 ($ACE1^{T65}$) has been reported as *OsSIN* (*Oryza sativa SHORT INTERNODE*)[57]. *OsSIN* has a 1 bp insertion at the same location as $ACE1^{T65}$. Han *et al.*[57] reported that constitutive expression of *OsSIN* ($ACE1^{T65}$) indicated dwarfism, but we did not observe a dwarf phenotype in T65 background. This may due to

792 differences in the genetic background. **d**, Amino acid sequences of long and short ACE1 proteins in
793 T65 and C9285. The short ACE1 protein was identical in T65 and C9285. **e**, Gross morphology of
794 *ACE1*$^{T65}$ and *ACE1*$^{C9285}$ overexpressors in T65 genetic background ($T_1$) under mock and GA treatment.
795 Transgenic plants were treated with $10^{-4}$ M $GA_3$ for 3 weeks after germination. Bars, 5 cm.
796 Arrowheads, nodes linked by elongated internodes. **f**, Quantitative data of the total internode length of
797 **(e)**. Data are means ± SD (n = 10 plants). One-way ANOVA followed by Tukey's multiple-comparison
798 test. **g**, Quantification of *OsMADS14* and *OsMADS15* expression in control and *ACE1*$^{C9285}$
799 overexpressor plants ($T_1$) under mock or GA treatment. Data are means ± SD (n = 4 plants). One-way
800 ANOVA followed by Tukey's multiple-comparison test. T65 at the vegetative (5-LS) and reproductive
801 (12-LS) phases were used as controls. GA was applied to 6-leaf-stage plants for 1 week. RNA was
802 extracted from a ~1 cm region of the shoot apex including the shoot apical meristem, developing leaves,
803 and internodes. Because the *ACE1*$^{C9285}$ overexpressor plants did not express *OsMADS14* and
804 *OsMADS15*, they were in the vegetative phase. **h**, Gross morphology of *ACE*$^{C9285}$ and *ACE1*$^{short}$
805 overexpressors in T65 genetic background ($T_0$) under mock and GA treatment. Right upper panel
806 shows enlarged view of base of the plant. **i**, Quantitative data of the total internode length of **(h)**. GA
807 was applied for 2 weeks. Data are means ± SD. The number of plants is showed in the panel. One-way
808 ANOVA followed by Tukey's multiple-comparison test. **j,** Total internode length of *ACE1*
809 overexpressor in NIL12 genetic background ($T_0$) without GA treatment. Data are means ± SD. The
810 number of plants is showed in the panel. One-way ANOVA followed by Tukey's multiple-comparison
811 test. **k**, Gross morphology (upper panels) and enlarged view (lower panels) of the vector control and
812 *ACE1*$^{C9285}$ overexpressor in the NIL1+3+12 genetic background. Bars, 10 cm. **l and m**, Total internode
813 length (**l**) and number of elongated internodes (**m**) of **k**. Data are means ± SD. The number of plants
814 is showed in the panel. Numbers indicate *P* values derived from a two-tailed *t*-test. **n**, Gross

morphology (left panel) and enlarged view (right panel) of the *ACE1*$^{C9285}$ overexpressor ($T_0$) in C9285 genetic background. Arrowheads indicate nodes linked by elongated internodes. Bars, 10 cm. The creeping-like stem elongation is likely to be due to rapid stem elongation that cannot support shoot weight; therefore, internodes bend and touch the ground. All experiments were repeated two times with similar results.

**Extended Data Figure 5. Quantification of *ACE1* expression in plant tissues**.

**a**, Schematic diagram of a rice plant showing the organs from which RNA was extracted to assess *ACE1* expression. Total RNA was extracted from roots, leaf sheath (LS), youngest fully expanded leaf blade (LB), elongating leaf blade (ELB), shoot apex (SA), and elongating internode. The internode was sampled separately at the base (lower) and middle part of the internode (middle). **b**, Quantification of *ACE1* expression under shallow water (SW) and deepwater (DW) conditions. DW conditions were maintained for 1 week. Data are means ± SD (n = 3 plants). Numbers indicate *P* values derived from a two-tailed *t*-test. **c to f**, Quantification of expression of cell elongation-related genes, *OsEXPA4* and *OsEXPB4*, and cell division-related genes, *CDKA1* and *CyclinB2;1*, in internode under shallow water (SW) or deepwater (DW) conditions. Data are means ± SD (n = 3 plants). One-way ANOVA followed by Tukey's multiple-comparison test. Cell elongation-related genes showed higher expression in the middle region while cell division-related genes showed higher expression in the lower region. These results suggest *ACE1* is preferentially expressed in cell elongation zone (middle region) rather than cell division zone (lower region). DW treatment was conducted for 1 week. All experiments were repeated two times with similar results.

**Extended Data Figure 6. Screening of transactivating factors of the *ACE1* promoter.**

**a**, Trans-eQTL region of *ACE1* on chromosome 9. The genome-wide eQTL mapping identified 7,145 significant trans-eQTLs (false discovery rate < 0.05) using the R/qtl[32] and R/eqtl packages[33]. The

genotype and expression data were derived from Kuroha *et al*.[31](85 individuals of the T65/Bhadua RILs). Of these, we detected one *trans* regulatory region on chromosome 9 as a trans-eQTL (limit of detection, 2.5; maximum limit of detection peak marker, ad09003568) that regulates the expression of *ACE1* (Os03g0346200). In this analysis, we used a support interval of 1.5 and the default settings in the R/eqtl::define.peak() function to evaluate QTLs and support intervals. **b**, Expression of transcription factor genes in the trans-eQTL region. Among the genes included in the overlapping region of trans-eQTL and GA-related QTL analyses, eight transcription factor genes were selected from the RNA sequence data of Minami *et al*.[58]. Data are means ± SD (n = 3 plants). The expression of *Os09t0306400* (*bZIP71*), *Os09g0287000* (*SUB1B*), and *Os09g0286600* (*SUB1C*) was altered under DW conditions. These genes were used as effectors in the transactivation analysis. **c,** About 4.7 kb upstream of the $ACE1^{T65}$-coding region and 4.4 kb upstream of the $ACE1^{C9285}$-coding region were amplified from genomic DNA of T65 and C9285 by PCR, respectively, and fused with *hRluc* (*Renilla reniformis*) in pUC19. These constructs were employed as reporters in the transactivation analysis. Black lines and colored charts indicate genomic sequences and sequence homologies, respectively. Sequence alignment was constructed by GenomeMatcher[59]. **d**, Screening of transactivating factors of the *ACE1* promoter using rice seeds. Constructs were introduced by bombardment. Data are means ± SD (n = 3 experiments). Numbers indicate *P* values derived from a two-tailed *t*-test when compared with VC. **e**, Effect of *SUB1C* overexpression on *ACE1* expression in T65 (left panel) and NIL3 (right panel). NIL3 possesses $ACE1^{C9285}$ in a T65 (see Extended Data Fig. 3e). X-axis, expression level of *SUB1C*; y-axis, expression level of *ACE1*. Dots indicate the expression levels of individual plants (n=6 plants). $R^2$, logarithmic approximation. **f**, Subcellular localization of SUB1C-GFP in onion epidermal cells**.** 35S:mCherry was used as a control. Fluorescence profiles were imaged by the profile tool of the ZEN software (Carl Zeiss). Plasmid constructs were introduced by particle bombardment. **g**,

Transactivation assay of *ACE1* promoter by SK1 and SK2. Data are means ± SD (n = 3 experiments). Numbers indicate *P* values derived from a two-tailed *t*-test when compared with VC. **h**, $ACE1^{T65}$-GFP and $ACE1^{C9285}$-GFP in onion epidermal cells. 35S:mCherry was used as a control. Fluorescence profiles were imaged by the profile tool of the ZEN software (Carl Zeiss). Plasmid constructs were introduced by particle bombardment. Nuclear localization signal (NLS) was predicted in $ACE1^{T65}$, but not in $ACE1^{C9285}$ by WOLF PSORT (https://www.genscript.com/wolf-psort.html). The GFP fluorescence signal of 35S:GFP and 35S:$ACE1^{C9285}$-GFP overlapped with mCherry signal, whereas 35S:$ACE1^{T65}$-GFP showed high intensity of GFP signal in the nucleus, suggesting that $ACE1^{T65}$ is preferentially localized in the nucleus. All experiments were repeated two times with similar results.

**Extended Data Figure 7. Tissue localization of ACE1 under GA treatment or DW conditions.**

**a**, Validation of an antibody against ACE1. Western-blot analysis using anti-GST (left) and anti-ACE1 (middle) antibodies after SDS–PAGE of crude protein extracts from *E. coli* including GST-ACE1 inducing construct. GST-ACE1 protein producing was induced by adding 1 mM isopropyl-1-thio-β-d-galactopyranoside (IPTG). Arrow indicates the position of GST-ACE1. CBB staining, loading control (right). **b**, Schematic diagram of internode. **c**, Immunostaining of ACE1 (red) in C9285 under GA treatment for 10 days. **d and e**, Enlarged views of red and yellow dashed square of **c**. **f to i**, Tissue localization of ACE1 under SW and DW conditions. Deepwater (DW) treatment was conducted for 1 day **(g)** and 10 days **(h)**, and compared with shallow water (SW) treatment **(f)**. **i**, Enlarged view of red dashed square in **h**. ACE1 signal was localized throughout the internode, except up to about 2 mm above the node, in early stage, and subsequently, it was detected from about 2 - 5 mm above the node 10 days later, whereas it was hardly detected about 10 mm above from node **(d and h)**. Bars, 1 mm. All experiments were repeated three times with similar results.

**Extended Data Figure 8. ACE1 function relates to intercalary meristem activity in concert with GA.**

**a**, Schematic diagram of internodes from which histological observations and mRNA expression analysis were conducted in **b to e**. EdU signal (green dots) at the shoot apex (**b**) and lower part (**c**) of an elongating internode of C9285 under SW conditions. **d**, Enlarged view of red dashed square in **c**. **e**, Expression of cell division-related genes, *Histone H4*, *CDKA1* and *CyclinB2;1,* at the SA and upper and lower elongating internodes under SW conditions. Data are means ± SD (n = 3 plants). Numbers indicate *P* values derived from a two-tailed *t*-test when compared with upper and lower. The EdU-positive region matches the area of expression of cell division-related genes. **f,** Visualization of cell division zone in VC and *ACE1*$^{C9285}$ox by EdU. The sixth internodes of 5-LS plants are highlighted (red arrows). $10^{-4}$ M $GA_3$ treatment was conducted for 0, 3, 5, and 10 days. Bars, 1 mm. **g**, Time-dependent changes in internode length of VC and *ACE1*$^{C9285}$ox in T65 genetic background in response to GA treatment. Right panel, enlarged view of the data from 0 to 5 days. Data are means ± SD. The number of plants is showed in the panel. Numbers indicate *P* values derived from a two-tailed *t*-test when compared with VC. All experiments were repeated three times with similar results. **h**, Model of internode GA response in the absence of ACE1. Cell division occurs during internode development without ACE1. However, competency for the GA response cannot be acquired by this internode, hence, the intercalary meristem does not develop or meristem activity may not be continued, and internodes are differentiated, in the presence of GA. **i**, Model of internode GA response in the presence of ACE1. ACE1 confers competence for GA response in the internode to develop intercalary meristem. Subsequently, intercalary meristem activity and its maintenance in internodes increases in concert with GA, resulting in the initiation of internode elongation. Interestingly, although *ACE1*$^{C9285}$ expression was highest at cell elongation zone, 10 - 30 mm from the node (Extended Data Figure 5b), ACE1$^{C9285}$

protein was detected in the region 2 - 5 mm from the node under GA treatment and DW condition for 10 days (Fig. 3a-d, Extended Data Figure 7, which coincided with the region where the EdU signal was detected (Extended Data Figure 8). In addition, overexpression of *ACE1*$^{C9285}$ induced cell division in coordination with GA in the basal region of elongating internode (Figure 3e). These results suggest that the protein stability of ACE1$^{C9285}$ may increase at intercalary meristem, or mRNA or protein is transported and accumulated in this region to control intercalary meristem activity. Previously, it has been proposed that the cell cycle entry at intercalary meristem might be a consequence of GA-induced cell elongation, since cell elongation of deepwater rice internode occurred prior to cell division under GA treatment[3,60]. The high expression of *ACE1* in the cell elongation zone above intercalary meristem may suggest that ACE1 is a regulatory molecule that controls cell division by transmitting cell elongation signals to intercalary meristem in GA-dependent manner. Further verifications such as changes in subcellular localization by GA treatment, RNA/protein stability or mobility, and identification of downstream targets of ACE1 are required to understand the mechanism of the molecular function.

**Extended Data Figure 9. Role of *ACE1-like1* in normal paddy rice.**

**a**, Phylogenetic tree constructed using the full-length amino acid sequences of ACE1 homologs from Phytozome (https://phytozome.jgi.doe.gov/pz/portal.html) using MEGA 7. Numbers on branches are the 1000-bootstrap values. **b**, The model of ACE1$^{C9285}$ protein sequence. The numbers indicate the amino acid positions. ACE1$^{C9285}$ and homologs possess three motifs of unknown function (Supplementary Table 2). **c to d**, A phylogenetic tree of ACE1 homologs in the mosses, pteridophytes (**c**), dicotyledon subgroup I clade **(d)** and dicotyledon subgroup II clade (**e**) in **a**. Dicotyledon subgroup I contains FPF1[17], an *Arabidopsis* homolog of ACE1. Dicotyledonous and monocotyledonous ACE1 homologs formed individual clades without mixing. Numbers on branches are the 1000-bootstrap

values. **f**, Overexpression of *Arabidopsis FPF1* in T65 genetic background ($T_0$). Upper panel, gross morphology of the vector control, *ACE1*$^{C9285}$ overexpressor, and *FPF1* overexpressor in the T65 genetic background. *FPF1* was cloned from a Col-0 plant. GA treatment was performed for 2 weeks. Arrowheads indicate nodes linked by elongated internodes. Bars, 1 cm. Lower, total internode length. Data are means ± SD. The number of plants is showed in the panel. One-way ANOVA followed by Tukey's multiple-comparison test. *Arabidopsis FPF1* was overexpressed in rice; however, it did not induce internode elongation, suggesting that *ACE1* and *FPF1* have distinct functions in rice and *Arabidopsis*, respectively. **g**, Sequence alignment of ACE1 homologs in rice. Among the six rice homologs, *ACE1* had the highest homology with *LOC_Os07g47450*, and we named it *ACE1-LIKE1* (*ACL1*). Although *LOC_Os01g15340* has been termed *ROOT ARCHITECTURE ASSOCIATED1* (*RAA1*)[61], its involvement in internode elongation has not been reported. **h**, Quantification of *OsMADS14*, *OsMADS15***,** and *ACL1* expression at each leaf stage in Nipponbare under shallow-water conditions. Data are means ± SD (n = 4 plants). One-way ANOVA followed by Tukey's multiple-comparison test. **i**, Sequence of the *acl1* mutant generated using the CRISPR/Cas9 system. **j**, Gross morphology of the wild-type (WT) and the *acl1* mutants at mature stage. Bars, 1 m. **k**, Quantitative data of **(j)**. The number of plants is showed in the panel. One-way ANOVA followed by Tukey's multiple-comparison test. All experiments were repeated two times with similar results.

**Extended Data Figure 10. The role of *ACE1* in Gramineae.**

**a**, Gross morphology of *ACE1*$^{C9285}$ overexpressors in *Brachypodium distachyon* without GA treatment after ripening. Bars, 5cm. **b**, Quantification of *ACE1* expression in *ACE1* overexpressors in *B. distachyon*. Data are means ± SD (n = 4 plants). Numbers indicate *P* values derived from a two-tailed t-test when compared with VC. **c and d**, Total internode length of *ACE1* overexpressors in *B. distachyon* under mock (**c**) or GA treatment (**d**). Data are means ± SD (n = 5 plants). Numbers indicate

*P* values derived from a two-tailed t-test when compared with VC. GA treatment was performed on the plants 1 week after germination for 3 weeks. **e**, Gross morphology of *ACE1*-RNAi in *B. distachyon* without (left) and with (right) GA treatment. Numbers below the photographs represent independent $T_0$ lines. Bars, 5 cm. **f**, Sequence alignment of ACE1 homologs of *B. distachyon*. Red arrows indicate the positions of primers for detection of the expression of endogenous *ACE1* homologs. **g**, Expression of *ACE1* homologs in *B. distachyon* in VC and *ACE1*-RNAi lines (n = 4 plants). **h and i**, Total internode length without (**h,** n = 9 plants) and with (**i,** n = 10 plants) GA treatment. Data are means ± SD and numbers indicate *P* values derived from a two-tailed *t*-test when compared with VC (**g** to **i**). One week after seed germination, plants were treated with GA for 3 weeks. **j**, Gross morphology of vector control and $ACE1^{C9285}$ox in barley under mock condition. Right panels show enlarged views of internodes. Arrowheads indicate the positions of nodes. **k**, Expression of *ACE1* in VC and of $ACE1^{C9285}$ox in barley (n = 4 plants). Number indicates *P* value derived from a two-tailed *t*-test. **l and m**, Total internode length **(l),** and number of elongated internodes **(m)** in transgenic barley plants overexpressing $ACE1^{C9285}$ox. Data are means ± SD (n = 6 plants). One-way ANOVA followed by Tukey's multiple-comparison test. There were significant differences in total internode length and number of elongated internodes. Plastochrons were not affected by $ACE1^{C9285}$ox, suggesting that initiation of internode elongation is promoted in plants overexpressing $ACE1^{C9285}$ox. **n**, Schematic diagram of plant growth of sugarcane and GA treatment. After excising the leaves of the $T_0$ plant, the elongated internode was cut into 3 cm pieces, which included a node (left). Cut internodes were divided into two and planted in soil. Plants with two or three developed leaves were subjected to mock or GA treatment for 4 weeks (right). **o**, Expression of *ACE1* in VC and of $ACE1^{C9285}$ox in sugarcane. Data are means ± SD (n = 4 plants). Number indicates *P* value derived from a two-tailed t-test. **p**, Total internode length and number of elongated internodes in transgenic sugarcane plants overexpressing

*ACE1*$^{C9285}$ox. Data are means ± SD. Numbers indicate *P* values derived from a two-tailed t-test in -GA or +GA. The number of elongated internodes differed significantly between the control and *ACE1*$^{C9285}$ox under mock and GA treatments. **q**, Sequence alignment of ACE1 homologs in sugarcane. Sequences were obtained from Sugarcane Genome Hub (https://sugarcane-genome.cirad.fr). All experiments were repeated two times with similar results.

**Extended Data Figure 11. The identification of the causal gene in the QTL on chromosome 12 in response to GA.**

**a**, Total internode length of *SK1* and *SK2* overexpressors after maturation. Dots indicate the total internode lengths of individual plants. Data are means ± SD. The number of plants is showed in the panel. One-way ANOVA followed by Tukey's multiple-comparison test. **b**, Genotype of the candidate region on chromosome 12. The mapping population generated by crossing NIL3+12 and NIL3 possessed a C9285 homozygote on chromosome 3. We previously identified roles for *SK1* and *SK2* on chromosome 12 in the deepwater (DW) response; however, positional cloning in response to GA excluded *SK* genes. Red arrow, candidate region of the GA response. T65-Homo, Hetero, and C9285-Homo indicate T65-type homozygous, heterozygous, and C9285-type homozygous genotypes, respectively, of the candidate region. **c**, Total internode length of each genotype after 3 weeks of GA treatment from germination. Data are means ± SD. The number of plants is showed in the panel. One-way ANOVA followed by Tukey's multiple-comparison test. **d**, Length of each internode. Ordinal number, internode position after germination. Data are means ± SD. The number of plants is showed in the panel. One-way ANOVA followed by Tukey's multiple-comparison test. **e and f**, Expression levels of candidate genes before (0 h) or after 24 h of $10^{-4}$ M $GA_3$ treatment. Data are means ± SD (n = 3 plants). One-way ANOVA followed by Tukey's multiple-comparison test. **g**, Gross morphology of vector control (VC) and *LOC_Os12g42250* (*DEC1*$^{T65}$)-ox in T65 genetic background after the

heading stage. Right panels show enlarged views of internodes and basal region of *LOC_Os12g42250* (*DEC1*$^{T65}$)-ox (dashed square). The number of non-elongated internodes increased, and internode length decreased, in *LOC_Os12g42250* (*DEC1*$^{T65}$)-ox, resulting in a reduction in total internode length. **h**, Effect of *LOC_Os12g42250* (*DEC1*$^{T65}$)-ox expression in T65 genetic background on total internode length. Y-axis, expression level of *LOC_Os12g42250* (*DEC1*$^{T65}$)-ox; x-axis, total internode length. Dots indicate individual plants (n = 5 plants). Right panel shows an enlarged view of the dashed square in the left panel. Plants with high *LOC_Os12g42250* (*DEC1*$^{T65}$)-ox expression showed a tendency to have a shorter plant height. **i**, Gross morphology of the *LOC_Os12g42260* overexpressor in NIL12 background ($T_0$). Arrowheads indicate the positions of nodes. One-month-old plants were treated with GA for 2 weeks. Bars, 10 cm. Right panel, internode length of the *LOC_Os12g42260* overexpressor in NIL12 genetic background ($T_0$). Data are means ± SD. The number of plants is showed in the panel. One-way ANOVA followed by Tukey's multiple-comparison test. **j**, Coding sequences of T65 *DEC1* and C9285 *DEC1*. **k**, Amino acid sequences of T65 DEC1 and C9285 DEC1. Green and red lines, LxLxL-type EAR motif and C2H2 zinc-finger domain, respectively. **l**, Gross morphology of the control plant and *LOC_Os12g42250* (*dec1*) mutant generated by CRISPR/Cas9 in NIL12 background ($T_0$) in the absence of GA. Arrowheads indicate the positions of nodes. Bars, 10 cm. **m**, Expression level of *DEC1*, *OsMADS14*, and *OsMADS15* at each growth stage of Nipponbare. Data are means ± SD (n = 4 plants). Numbers indicate *P* values derived from a two-tailed *t*-test when compared with the 4-LS. *OsMADS14* and *OsMADS15* were expressed at the 8-LS, whereas *DEC1* expression began to decrease at the 8-LS in Nipponbare. All experiments were repeated two times with similar results.

**Extended Data Figure 12. Expression level, subcellular localization, and transcriptional activity of DEC1.**

**a**, Schematic diagram of elongating internode of C9285 under SW (left) and DW (right) conditions. DW treatment was conducted for 24 h. Numbers next to internodes indicate the sampling positions and corresponding distances from point 1 (0–0.5 cm), the node at the base of the axillary bud; 2, 0.5–1.0 cm; 3, 1.0–1.5 cm; 4, 1.5–3.0 cm; 5, 3.0–4.0 cm from position 1. Point 6 is 4.5 cm – 6.0 cm in SW conditions, and 7.5 – 9.0 cm in DW conditions from position 1, respectively. Right panels, expression of *DEC1* and the cell division-related genes, *Histone H4* and *CDKA1*. *DEC1* was highly expressed in the cell division zone at around positions 2 and 3 under SW conditions but was downregulated under DW conditions. In contrast, the expression of cell division-related genes was increased at positions 2 and 3 under DW conditions. Data are means ± SD (n = 3 plants). **b**, Phylogenetic tree of DEC1 homologs constructed using the SALAD database (https://salad.dna.affrc.go.jp/salad/en/). **c**, Diagram of conserved motifs constructed using the SALAD database and the DEC1 sequence. Boxes and numbers represent conserved motifs. **d**, Conserved sequence of motif number 8 in **(c)**. This motif contains an LxLxL-type EAR motif. **e**, Conserved sequence of motif number 1 in **(c)**. This motif contains a C2H2-type zinc-finger domain. **f**, Conserved sequence of motif number 8 in **(c)**. This motif contains an LxLxL-type EAR motif. Conserved motifs were detected by WebLogo (http://weblogo.berkeley.edu). **g**, Subcellular localization of GFP, DEC1$^{T65}$-GFP and DEC1$^{C9285}$-GFP in onion epidermal cells. The signal of 35S:mCherry was used as a control. In profile of fluorescence, the GFP signal of 35S:GFP overlapped with mCherry signal, whereas 35S:DEC1$^{T65}$-GFP and 35S:DEC1$^{C9285}$-GFP showed high intensity of GFP signal in the nuclei, suggesting that DEC1$^{T65}$ and DEC1$^{C9285}$ are localized in the nuclei. Fluorescence profiles were imaged by the profile tool of the ZEN software (Carl Zeiss). Plasmid constructs were introduced by particle bombardment. **h**, Transcriptional activity of DEC1 by yeast one-hybrid assay. Left, diagrams of effector constructs. All experiments were repeated two times with similar results.

**Extended Data Figure 13. The effect of *DEC1* on internode elongation.**

**a**, Gross morphology of vector control, *DEC1*$^{T65}$ overexpressor (*DEC1*$^{T65}$ox), and *DEC1*$^{C9285}$ overexpressor (*DEC1*$^{C9285}$ox) in barley. Right panels show an enlarged view of the basal region of *DEC1*$^{T65}$ox and *DEC1*$^{C9285}$ox. Arrow indicates the position of the shoot apex. **b to d,** *DEC1* expression **(b)**, plant height **(c),** and total internode length **(d)** of transgenic barley plants overexpressing *DEC1*. Data are means ± SD (n = 4 plants). One-way ANOVA followed by Tukey's multiple-comparison test. **e**, Internode length of *dec1* mutant ($T_1$). Internodes of 5-leaf-stage plants of VC and *dec1* mutant were measured after 3 and 10 days of $10^{-4}$ M $GA_3$ treatment. Data are means ± SD (n = 6 plants). Numbers indicate *P* values derived from a two-tailed t-test when compared with total internode length of Mock control. **f and g**, EdU signal in the *dec1* mutant under mock or GA treatment for 3 days **(f)** and 10 days **(g)**. The fifth internodes of 5-leaf stage plants are highlighted **(f)**. An EdU signal was detected at the basal region of elongating internodes after 10 days of GA treatment **(g). h**, Expression of *ACE1* and *DEC1* in *ACE1*$^{C9285}$ox and the *dec1* mutant in T65 genetic background. Data are means ± SD (n = 4 plants). One-way ANOVA followed by Tukey's multiple-comparison test. **i and j,** Effect of *SK*s overexpression on *ACE1* and *DEC1* expression in NIL1+3+12. To examine the effect of *SK*s on *ACE1* and *DEC1* expression, *SK*s were overexpressed in NIL1+3+12 possessing C9285-type *ACE1* and *DEC1*. *SK*ox plants were grown under SW conditions. **i**, Expression of *SK1*, *SK2*, *ACE1* and *DEC1* in *SK*ox/NIL1+3+12 and C9285 under SW and DW conditions Data are means ± SD (n = 3 plants). **j**, Total internode length of *SK*ox plants under SW conditions. Data are means ± SD (n = 3 plants). Numbers indicate *P* values derived from a two-tailed *t*-test when compared with VC (**i and j)**. All experiments were repeated two times with similar results.

**Extended Data Figure 14. The selection of *ACE1* and *DEC1*, and application for breeding.**

**a**, Multiple regression of ACE1 and DEC1 in 28 individuals of O. rufipogon by generalized linear model (GLM) regression analysis. The two-sided p-value of a test on the null hypothesis of that the coefficient is equal to zero (no effect), was calculated with *F*-test which describes the ratio of two chi-squared distributed variables. **b**, Transition of EHH from the C9285-like (red) and T65-like (blue) haplotypes of *DEC1*, in 28 *O. rufipogon*. The two-sided p-value of a test on the null hypothesis of no selection from each core SNP was calculated from the Z-scores of the iHS values in chromosome 12 using the cumulative probability density function of the normal distribution. **c and d**, Comparison of allele frequencies of *DEC1* **(c)** and *ACE1* **(d)**, in *O. rufipogon* and six subpopulations of *O. sativa*. **e**, Genotypes of T65 and NIL1+3+12. NIL1+3+12 possesses QTL regions on chromosomes 1, 3, and 12 for the DW response in T65 genetic background. **f**, Gross morphology of T65 and NIL1+3+12. Two-month old plants were treated SW or DW treatment. During DW treatment, the water level was increased by 10 cm per day until a depth of 120 cm was achieved and continued until seed maturation (about 3 months). The water depth of SW conditions was 5 cm from the soil surface. **g and h**, Internode length after ripening (**g**), and number of grains per panicle (**h**). Data are means ± SD. The number of plants is showed in the panel. One-way ANOVA followed by Tukey's multiple-comparison test. T65 died under DW conditions within 3 months and was non-quantifiable **(g and h)**. All experiments were repeated two times with similar results. **i**, Schematic of the antagonistic regulatory mechanism of internode elongation by ACE1/ACL1 and DEC1. Upper panel and lower panels are models for normal paddy rice and DW rice, respectively.

## References

23. Kojima, M. *et al.* Highly sensitive and high-throughput analysis of plant hormones using MS-probe modification and liquid chromatography-tandem mass spectrometry: An application for hormone profiling in *Oryza sativa*. *Plant Cell Physiol.* **50**, 1201–1214 (2009).
24. Shinozaki, Y. *et al.* Ethylene suppresses tomato (*Solanum lycopersicum*) fruit set through modification of gibberellin metabolism. *Plant J.* **83**, 237–251 (2015).
25. Minami, A. *et al.* Cold acclimation in bryophytes: Low-temperature-induced freezing tolerance in Physcomitrella patens is associated with increases in expression levels of stress-related genes but not with increase in level of endogenous abscisic acid. *Planta* **220**, 414–423 (2005).
26. Ueguchi-Tanaka, M. *et al.* Molecular interactions of a soluble gibberellin receptor, GID1, with a rice DELLA protein, SLR1, and gibberellin. *Plant Cell* **19**, 2140–2155 (2007).
27. Zhang, H.-B., Zhao, X., Ding, X., Paterson, A. H. & Wing, R. A. Preparation of megabase-size DNA from plant nuclei. *Plant J.* **7**, 175–184 (1995).
28. International Rice Genome Sequencing Project. The map-based sequence of the rice genome. *Nature* **436**, 793–800 (2005).
29. Mikami, M., Toki, S. & Endo, M. Comparison of CRISPR/Cas9 expression constructs for efficient targeted mutagenesis in rice. *Plant Mol. Biol.* **88**, 561–572 (2015).
30. Hiei, Y., Ohta, S., Komari, T. & Kumashiro, T. Efficient transformation of rice (*Oryza sativa* L.) mediated by Agrobacterium and sequence analysis of the boundaries of the T-DNA. *Plant J.* **6**, 271–282 (1994).
31. Kuroha, T. *et al.* eQTLs regulating transcript variations associated with rapid internode elongation in deepwater rice. *Front. Plant Sci.* **8**, 1–16 (2017).
32. Arends, D., Prins, P., Jansen, R. C. & Broman, K. W. R/qtl: High-throughput multiple QTL mapping. *Bioinformatics* **26**, 2990–2992 (2010).
33. Cubillos, F. A. *et al.* Expression variation in connected recombinant populations of *Arabidopsis thaliana* highlights distinct transcriptome architectures. *BMC Genomics* **13**, 1–12 (2012).
34. Yamaji, N. & Ma, J. F. Spatial distribution and temporal variation of the rice silicon transporter Lsi1. *Plant Physiol.* **143**, 1306–1313 (2007).
35. Himuro, Y. *et al. Arabidopsis* galactinol synthase *AtGolS2* improves drought tolerance in the monocot model *Brachypodium distachyon*. *J. Plant Physiol.* **171**, 1127–1131 (2014).
36. Alves, S. C. *et al.* A protocol for *Agrobacterium*-mediated transformation of *Brachypodium distachyon* community standard line Bd21. *Nat. Protoc.* **4**, 638–649 (2009).
37. Hisano, H. & Sato, K. Genomic regions responsible for amenability to Agrobacterium-mediated transformation in barley. *Sci. Rep.* **6**, 1–11 (2016).

38. Takahashi, W. & Takamizo, T. Plant regeneration from embryogenic calli of the wild sugarcane (*Saccharum spontaneum* L .) clone ‘ Glagah Kloet ’. *Bull NARO Inst Livest Grassl Sci No.13* **13**, 23–32 (2013).
39. Takahashi, W., Oishi, H., Ebina, M., Takamizu, T. & Komatsu, T. Production of transgenic italian ryegrass (*Lolium multiflorum* Lam.) via microprojectile bombardment of embryogenic calli. *Plant Biotechnol.* **19**, 241–249 (2002).
40. Spangenberg, G. *et al.* Transgenic tall fescue (*Festuca arundinacea*) and red fescue (*F. rubra*) plants from microprojectile bombardment of embryogenic suspension cells. *J. Plant Physiol.* **145**, 693–701 (1995).
41. Li, H. & Durbin, R. Making the Leap: Maq to BWA. *Bioinformatics* **25**, 1754–1760 (2009).
42. Browning, B. L. & Browning, S. R. Genotype imputation with millions of reference samples. *Am. J. Hum. Genet.* **98**, 116–126 (2016).
43. Szpiech, Z. A. & Hernandez, R. D. Selscan: An efficient multithreaded program to perform EHH-based scans for positive selection. *Mol. Biol. Evol.* **31**, 2824–2827 (2014).
44. Sabeti, P. C. *et al.* Detecting recent positive selection in the human genome from haplotype structure. *Nature* **419**, 832–837 (2002).
45. Voight, B. F., Kudaravalli, S., Wen, X. & Pritchard, J. K. A map of recent positive selection in the human genome. *PLoS Biol.* **4**, 446–458 (2006).
46. Taoka, K. I. *et al.* 14-3-3 proteins act as intracellular receptors for rice Hd3a florigen. *Nature* **476**, 332–335 (2011).
47. Kobayashi, K. *et al.* Inflorescence meristem identity in rice is specified by overlapping functions of three *AP1/FUL*-Like MADS box genes and *PAP2*, a *SEPALLATA* MADS Box gene. *Plant Cell* **24**, 1848–1859 (2012).
48. Tsuji, H. *et al.* Hd3a promotes lateral branching in rice. *Plant J.* **82**, 256–266 (2015).
49. Kaneko-Suzuki, M. *et al.* TFL1-Like proteins in rice antagonize rice FT-Like protein in inflorescence development by competition for complex formation with 14-3-3 and FD. *Plant Cell Physiol.* **59**, 458–468 (2018).
50. Ikeda, A. *et al. slender* rice, a constitutive gibberellin response mutant, is caused by a null mutation of the *SLR1* gene, an ortholog of the height-regulating gene *GAI/RGA/RHT/D8*. *Plant Cell* **13**, 999–1010 (2001).
51. Fu, X. *et al.* Gibberellin-mediated proteasome-dependent degradation of the Barley DELLA protein SLN1 repressor. *Plant Cell* **14**, 3191–3200 (2002).
52. Hoffmann-Benning, S. & Kende, H. On the role of abscisic acid and gibberellin in the regulation of growth in rice. *Plant Physiol.* **99**, 1156–1161 (1992).

53. Azuma, T., Mihara, F., Uchida, N., Yasuda, T. & Yamaguchi, T. Plant hormonal regulation of internodal elongation of floating rice stem sections. *Japanese J. Trop. Agric.* **34**, 271–275 (1990).
54. Nemoto, K., Ukai, Y., Tang, D.-Q., Kasai, Y. & Morita, M. Inheritance of early elongation ability in floating rice revealed by diallel and QTL analyses. *Theor. Appl. Genet.* **109**, 42–47 (2004).
55. Tang, D.-Q., Kasai, Y., Miyamoto, N., Ukai, Y. & Nemoto, K. Comparison of QTLs for early elongation ability between two floating rice cultivars with a different phylogenetic origin. *Breed. Sci.* **55**, 1–5 (2005).
56. Kawano, R., Doi, K., Yasui, H., Mochizuki, T. & Yoshimura, A. Mapping of QTLs for floating ability in rice. *Breed. Sci.* **58**, 47–53 (2008).
57. Han, Y. *et al.* Overexpression of *OsSIN*, encoding a novel small protein, causes short internodes in Oryza sativa. *Plant Sci.* **169**, 487–495 (2005).
58. Minami, A. *et al.* Time-course transcriptomics analysis reveals key responses of submerged deepwater rice to flooding. *Plant Physiol.* **176**, 3081–3102 (2018).
59. Ohtsubo, Y., Ikeda-Ohtsubo, W., Nagata, Y. & Tsuda, M. GenomeMatcher: A graphical user interface for DNA sequence comparison. *BMC Bioinformatics* **9**, 1–9 (2008).
60. Sauter, M. & Kende, H. Gibberellin-induced growth and regulation of the cell division cycle in deepwater rice. *Planta* **188**, 362–368 (1992).
61. Ge, L., Chen, H., Jiang, J. & Zhao, Y. Overexpression of *OsRAA1* causes pleiotropic phenotypes in transgenic rice plants, including altered leaf, flower, and root development and root response to gravity. *Plant Physiol.* **135**, 1502–1513 (2004).

**Acknowledgments:** We thank Prof. Hiroko Morishima (deceased 2010) for encouragement to do this work and Kensuke Suzuki, Yuma Kondo, Masaya Koike, Anzu Minami, Stefan Reuscher, Naoki Yamaji, Jian Feng Ma and Sayaka Sasaki for technical assistance. We thank Masafumi Mikami, Seiichi Toki and Masaki Endo (NARO) for providing the CRISPR/Cas9 vectors. We thank Miyako Ueguchi-Tanaka for providing the SLR1 antibody. We thank Rosalyn B. Angeles-Shim for English-language editing. Deepwater rice, wild rice accessions, and barley cv. Golden Promise were provided by the National Bioresource Project (NBRP) of the Ministry of Education, Culture, Sports, Science and Technology (MEXT) of Japan.

**Funding:** This work was supported by the CREST program of the JST (no. JPMJCR13B1), by the SATREPS program (no. JPMJSA1706) of the JST and JICA, and by MEXT/JSPS KAKENHI (nos. 16K18565, 16H06466, 17H06473, and 19K15815). This study was supported in part by RIKEN-Nagoya University Science and Technology Hub.

**Authors' contributions:** K.N. and M.A. designed the study. K.N. and S.I. carried out the genetic linkage analysis. J.W. and T.F. performed the screening of bacterial artificial chromosome clones and sequence analysis. K.N., R.G., Y.N., M.F., Y.H., M.K., W.A., H.H., and K.S. performed the transgenic experiments and sequence analysis. K.N., Y.M., R.G., T.H., A.Y., and H.T. elucidated the molecular mechanisms. M.K., Y.T., and H.S. quantified the hormone levels. A.F. performed the trans-eQTL analysis. Y.S. and T.A. performed the evolutionary analyses. K.N., T.A., and M.A. wrote the manuscript.

**Competing interests:** The authors declare that they have no competing interests.

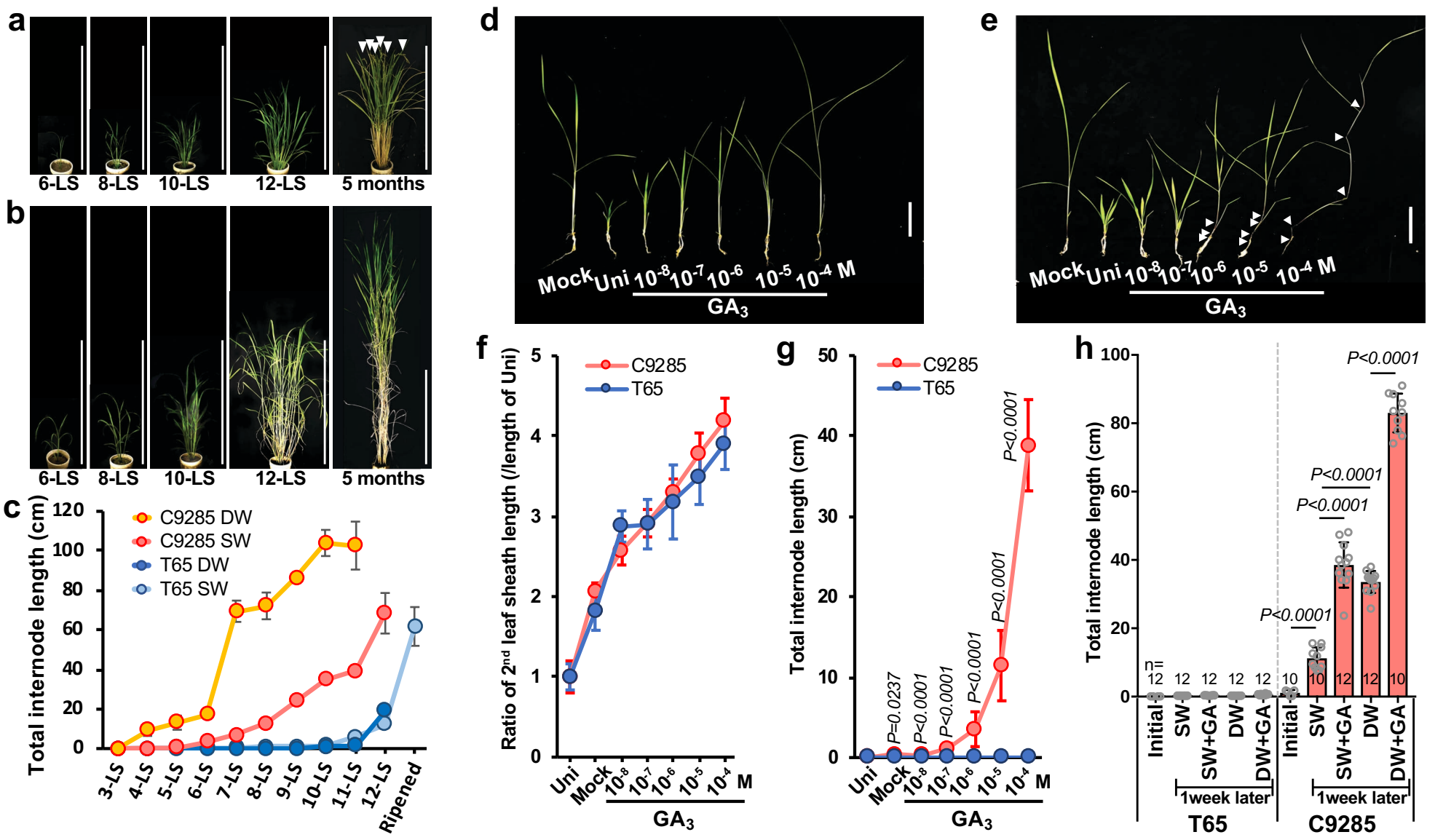
a
6-LS
8-LS
10-LS
12-LS
5 months
b
6-LS
8-LS
10-LS
12-LS
5 months
c
Total internode length (cm)
C9285 DW
C9285 SW
T65 DW
T65 SW
3-LS
4-LS
5-LS
6-LS
7-LS
8-LS
9-LS
10-LS
11-LS
12-LS
Ripened
d
Mock
Uni
10-8
10-7
10-6
10-5
10-4 M
GA3
e
Mock
Uni
10-8
10-7
10-6
10-5
10-4 M
GA3
f
Ratio of 2nd leaf sheath length (/length of Uni)
C9285
T65
Uni
Mock
10-8
10-7
10-6
10-5
10-4 M
GA3
g
Total internode length (cm)
C9285
T65
P=0.0237
P<0.0001
P<0.0001
P<0.0001
P<0.0001
P<0.0001
Uni
Mock
10-8
10-7
10-6
10-5
10-4 M
GA3
h
Total internode length (cm)
P<0.0001
P<0.0001
P<0.0001
P<0.0001
n=
12
12
12
12
12
10
10
12
12
10
Initial
SW
SW+GA
DW
DW+GA
Initial
SW
SW+GA
DW
DW+GA
1week later
1week later
T65
C9285

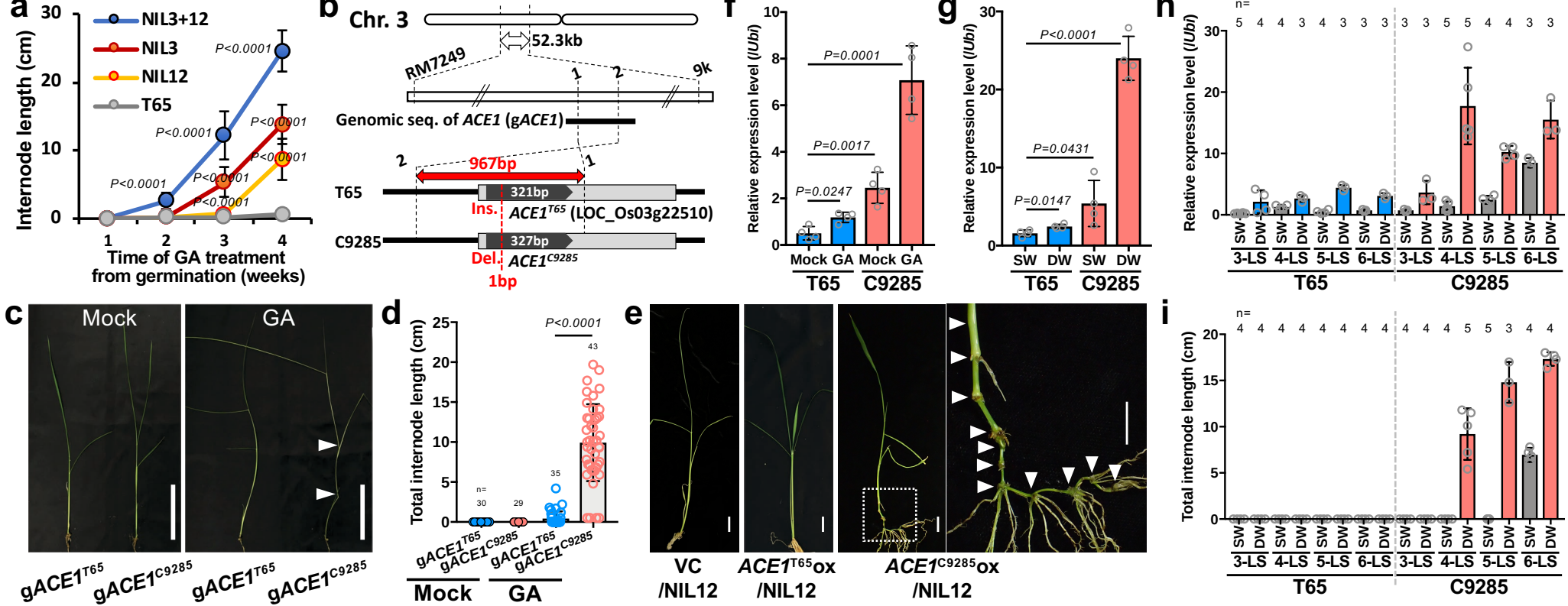
a
Internode length (cm)
Time of GA treatment from germination (weeks)
NIL3+12
NIL3
NIL12
T65
P<0.0001
b
Chr. 3
52.3kb
RM7249
9k
Genomic seq. of ACE1 (gACE1)
967bp
321bp
Ins.
ACE1T65 (LOC_Os03g22510)
327bp
Del.
ACE1C9285
1bp
T65
C9285
c
Mock
GA
gACE1T65
gACE1C9285
d
Total internode length (cm)
P<0.0001
Mock
GA
e
VC /NIL12
ACE1T65ox /NIL12
ACE1C9285ox /NIL12
f
Relative expression level (/Ubi)
P=0.0001
P=0.0017
P=0.0247
g
P<0.0001
P=0.0431
P=0.0147
h
n=
3-LS
4-LS
5-LS
6-LS
i

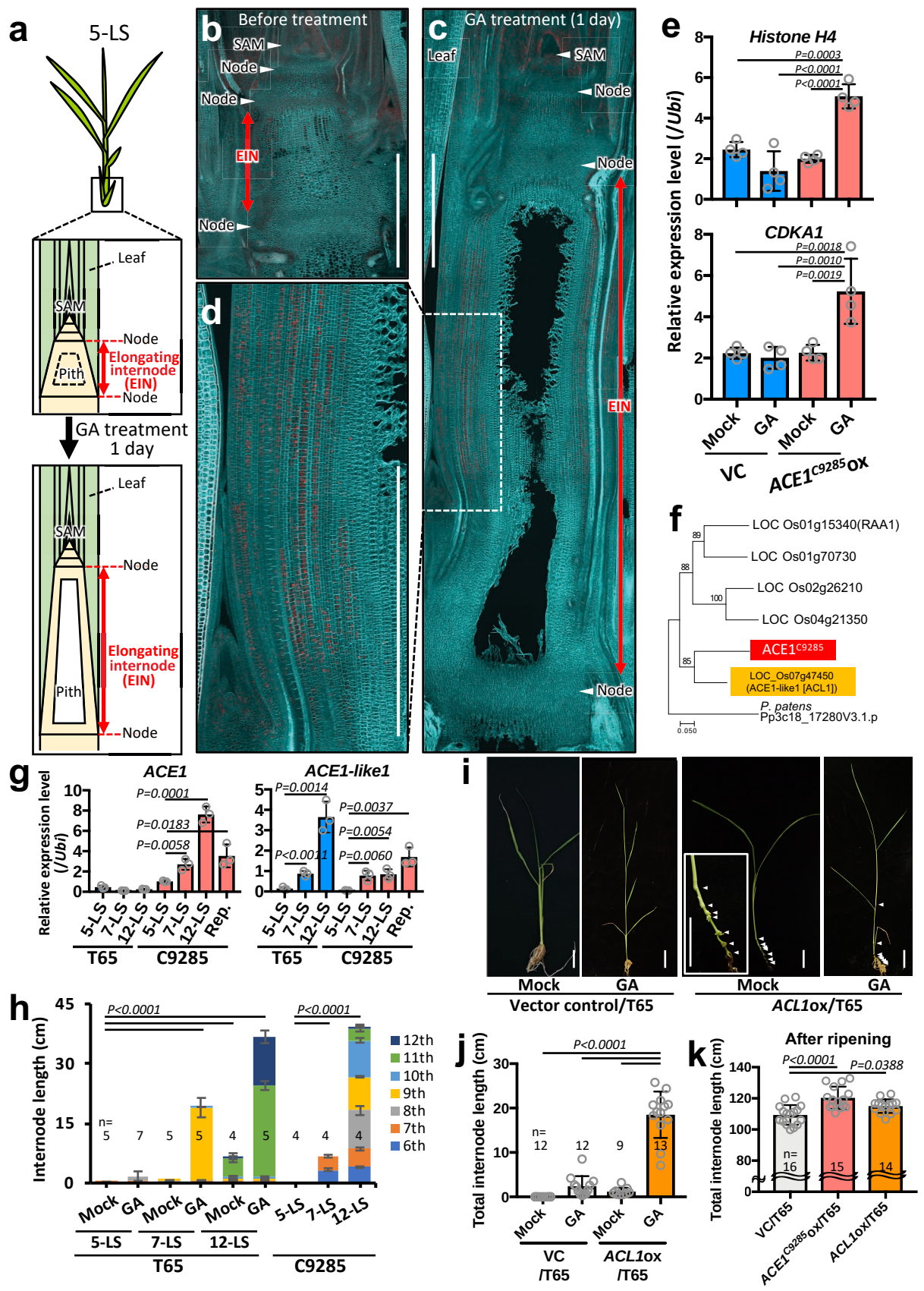
a
5-LS
Leaf
SAM
Node
Pith
Elongating internode (EIN)
Node
GA treatment 1 day
Leaf
SAM
Node
Elongating internode (EIN)
Pith
Node
b
Before treatment
SAM
Node
Node
EIN
Node
c
GA treatment (1 day)
Leaf
SAM
Node
Node
EIN
Node
d
e
Histone H4
P=0.0003
P<0.0001
P<0.0001
CDKA1
P=0.0018
P=0.0010
P=0.0019
Relative expression level (/Ubi)
Mock
GA
Mock
GA
VC
ACE1C9285ox
f
LOC Os01g15340(RAA1)
LOC Os01g70730
LOC Os02g26210
LOC Os04g21350
ACE1C9285
LOC_Os07g47450 (ACE1-like1 [ACL1])
P. patens Pp3c18_17280V3.1.p
89
88
100
85
0.050
g
ACE1
ACE1-like1
Relative expression level (/Ubi)
P=0.0001
P=0.0183
P=0.0058
P=0.0014
P<0.0011
P=0.0037
P=0.0054
P=0.0060
5-LS
7-LS
12-LS
5-LS
7-LS
12-LS
Rep.
T65
C9285
T65
C9285
i
Mock
GA
Mock
GA
Vector control/T65
ACL1ox/T65
h
Internode length (cm)
P<0.0001
P<0.0001
n=
5
7
5
5
4
5
4
4
4
12th
11th
10th
9th
8th
7th
6th
Mock
GA
Mock
GA
Mock
GA
5-LS
7-LS
12-LS
5-LS
7-LS
12-LS
T65
C9285
j
Total internode length (cm)
P<0.0001
n=
12
12
9
13
Mock
GA
Mock
GA
VC /T65
ACL1ox /T65
k
After ripening
Total internode length (cm)
P<0.0001
P=0.0388
n=
16
15
14
VC/T65
ACE1C9285ox/T65
ACL1ox/T65

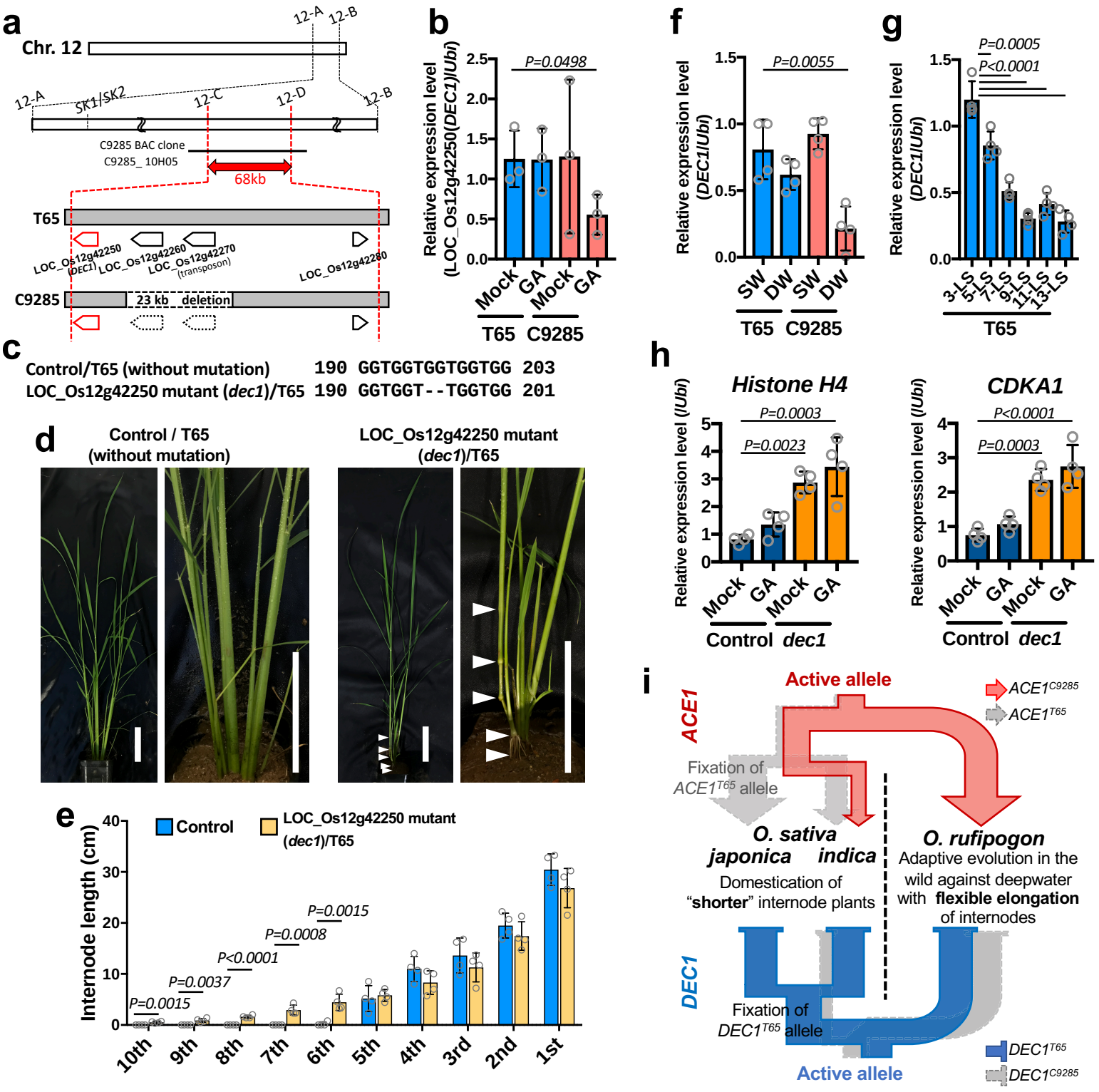
a
Chr. 12
12-A
12-B
12-A
SK1/SK2
12-C
12-D
12-B
C9285 BAC clone
C9285_ 10H05
68kb
T65
LOC_Os12g42250 (DEC1)
LOC_Os12g42260
LOC_Os12g42270 (transposon)
LOC_Os12g42280
C9285
23 kb deletion
b
Relative expression level (LOC_Os12g42250(DEC1)/Ubi)
P=0.0498
Mock
GA
Mock
GA
T65
C9285
f
Relative expression level (DEC1/Ubi)
P=0.0055
SW
DW
SW
DW
T65
C9285
g
Relative expression level (DEC1/Ubi)
P=0.0005
P<0.0001
3-LS
5-LS
7-LS
9-LS
11-LS
13-LS
T65
c
Control/T65 (without mutation) 190 GGTGGTGGTGGTGG 203
LOC_Os12g42250 mutant (dec1)/T65 190 GGTGGT--TGGTGG 201
d
Control / T65 (without mutation)
LOC_Os12g42250 mutant (dec1)/T65
e
Internode length (cm)
Control
LOC_Os12g42250 mutant (dec1)/T65
P=0.0015
P=0.0037
P<0.0001
P=0.0008
P=0.0015
10th
9th
8th
7th
6th
5th
4th
3rd
2nd
1st
h
Histone H4
Relative expression level (/Ubi)
P=0.0003
P=0.0023
Mock
GA
Mock
GA
Control
dec1
CDKA1
Relative expression level (/Ubi)
P<0.0001
P=0.0003
Mock
GA
Mock
GA
Control
dec1
i
ACE1
Active allele
ACE1C9285
ACE1T65
Fixation of ACE1T65 allele
O. sativa
japonica
indica
Domestication of "shorter" internode plants
O. rufipogon
Adaptive evolution in the wild against deepwater with flexible elongation of internodes
DEC1
Fixation of DEC1T65 allele
Active allele
DEC1T65
DEC1C9285